processes

MDPI

*Article*

# Impact of Substrate Type on the Properties of Cast Biodegradable Starch-Based Films

**Tomasz Tadeusz Murawski, Zuzanna Żołek-Tryznowska and Jerzy Szałapak ***

Institute of Mechanics and Printing, Faculty of Mechanical and Industrial Engineering, Warsaw University of Technology, 00-661 Warsaw, Poland; tomasz.murawski.dokt@pw.edu.pl (T.T.M.); zuzanna.tryznowska@pw.edu.pl (Z.Ż.-T.)
* Correspondence: jerzy.szalapak@pw.edu.pl

**Abstract:** Biodegradable films are a viable alternative to conventional plastics, thereby contributing to environmental pollution reduction. This study investigates the impact of substrate type on the properties of starch-based films produced using a plasticizer-assisted casting method. Four different substrates, namely, glass, copper, copper-free laminate, and Teflon®, were evaluated, addressing a research gap in which previous studies primarily focused on film composition. The films were analyzed for color, tensile strength, surface free energy, and surface morphology using optical and electron microscopy. The results demonstrated a substrate-dependent impact on surface properties, particularly optical transparency, surface roughness, and adhesion. The films cast on glass and laminate exhibited higher transparency and lower roughness, while copper substrate induced micro-striations and strong adhesion. Teflon® substrates replicated surface imperfections, which may be advantageous for optical applications, but caused film delamination. Tensile strength did not show statistically significant differences across substrates, although reduced elongation was observed for the films cast on Teflon®. Water vapor permeability was also not significantly affected, indicating a dominant role of bulk material properties. It averaged 25 kg per day per square meter, which means high vapor permeability. Surface free energy analysis revealed marked variations between top and bottom layers, with values ranging from 35 to 70 $mJ \cdot m^{-2}$ depending on the substrate. These findings confirm that the type of casting substrate plays a critical role in determining the surface and optical properties of starch-based films, even at the laboratory scale. This study provides new insights into substrate–film interactions and establishes a foundation for optimizing biodegradable film fabrication for industrial and application-specific needs.

**Keywords:** biodegradable films; starch-based films; film casting; substrate influence; surface properties; mechanical properties; optical properties; biodegradable films for packaging applications; packaging

check for updates

Academic Editor: Fabiano André Narciso Fernandes

Received: 28 February 2025
Revised: 31 March 2025
Accepted: 9 April 2025
Published: 15 April 2025

**Citation:** Murawski, T.T.; Żołek-Tryznowska, Z.; Szałapak, J. Impact of Substrate Type on the Properties of Cast Biodegradable Starch-Based Films. *Processes* **2025**, *13*, 1197. https://doi.org/10.3390/pr13041197

**Copyright:** © 2025 by the authors. Licensee MDPI, Basel, Switzerland. This article is an open access article distributed under the terms and conditions of the Creative Commons Attribution (CC BY) license (https://creativecommons.org/licenses/by/4.0/).

## 1. Introduction

Biodegradable films are a viable alternative to conventional packaging materials, especially in the food industry, where environmental issues play a key role. With the growing problem of plastic pollution and increasing environmental awareness among consumers [1], the search for sustainable food-packaging solutions is becoming a priority for many companies and researchers. Biodegradable films derived from natural polymers, such as polysaccharides (e.g., starch [1], chitosan [2,3], and cellulose [4]) and proteins (e.g., casein [5], gelatin [6], and soy [7]), show significant potential in reducing the environmental

impact of packaging. Due to their ability to degrade under natural conditions, they can reduce landfill waste and limit microplastic emissions to aquatic and soil ecosystems [8].

Beyond their environmental benefits, biodegradable films offer a wide range of applications not only by improving food preservation [2,3,9] but also by affecting the sanitary–epidemiological safety of products [6,10–12]. Additionally, some biodegradable coatings have gas-exchange-regulating properties. These coatings help regulate moisture and oxygen levels, which slows product spoilage [2]. In this way, food waste may be reduced, addressing one of the key challenges of the modern food industry [13].

The development and commercialization of biodegradable films are supported by numerous scientific studies and legislative initiatives promoting eco-friendly packaging solutions. A growing number of countries are introducing regulations restricting the use of conventional plastics, fostering a growing interest in environmentally friendly alternatives [14–16]. At the same time, the challenges of manufacturing costs and optimizing the mechanical properties of these materials remain the subject of intense research and development [9,10]. The following text highlights key applications of biodegradable films in packaging.

Biodegradable-packaging films play a key role in extending the shelf lives of food products. Due to their ability to incorporate natural antioxidants and antimicrobial agents, such as essential oils, these films effectively inhibit the growth of microorganisms, which is particularly crucial for perishable foods, especially meat [17–19].

Moisture control is another important aspect of food preservation. Films made of hemicellulose and cellulose derivatives are characterized by a lower moisture content, which promotes better storage conditions for food products [20,21].

The use of biodegradable packaging materials significantly contributes to reducing plastic waste. The use of polymers from natural sources reduces dependence on petrochemical-based plastics, which helps reduce environmental pollution [22].

In addition, films based on polysaccharides come from renewable sources, thereby supporting sustainable packaging solutions [23].

The mechanical strength of biodegradable films can be improved by adding plasticizers, such as glycerol or polyethylene glycol, to them. Such modifications increase the flexibility and durability of these films, expanding their range of applications in packaging [20].

In addition, developments in nanotechnology have enabled the creation of smart biodegradable packaging that can monitor food quality and safety. Such packaging may include indicators detecting changes in product quality, allowing for better freshness control [22].

Starch-based biodegradable films exhibit varied properties depending on several key factors, including the type and concentration of plasticizers, processing techniques, and reinforcing additives. Each of these elements plays a significant role in determining the mechanical strength, moisture resistance, and biodegradability of the films.

Plasticizers are essential in the production of starch-based films as they influence flexibility, mechanical strength, and structural stability.

Glycerol is the most commonly used plasticizer. Its concentration (20–80%) significantly affects a film's properties: a higher glycerol content generally increases flexibility but may reduce tensile strength. Studies have shown that the addition of glycerol increases intermolecular spacing, which enhances molecular mobility and decreases the crystallinity of a material [24].

Ultrasound treatment applied to films containing 20% and 40% glycerol resulted in a 20% increase in tensile strength, suggesting that specific processing methods can

optimize film performance [25]. Such treatment also improves the surface properties of polymer layers.

The method used to extract and gelatinize starch also affects the final film structure: optimizing processing parameters allows for the creation of layers with desirable thickness and density [26].

Incorporating appropriate additives into starch-based films can significantly improve their mechanical, barrier, and functional properties. Organic and inorganic nanoparticles enhance thermal stability, mechanical resistance, and barrier properties, making starch-based films more competitive compared to conventional plastics [27]. Also, the addition of antioxidants, such as dialdehyde starch and caffeic acid, not only improves mechanical strength but also imparts antioxidant properties, making films suitable for food packaging applications [28]. Such approaches align with recent research on thermoplastic starch composites reinforced with mineral fillers like micronized chalcedonite, which enhance mechanical performance without compromising biodegradability [29].

Recent studies in the literature have also demonstrated the potential of starch-based materials in printed electronics, including biodegradable sensors and QR-coded packaging [30–34]. Other polysaccharides, such as cellulose and chitosan, have been applied to improve food safety and environmental performance in smart packaging solutions [23]. In addition, biodegradable films show growing relevance in pharmaceutical applications as sustainable carriers for drug delivery [35,36].

Our previous research has explored various ways of enhancing starch films, including in regard to printability, the cytocompatibility of electroconductive composites, and the effect of fillers like silica on surface energy and mechanical behavior.

The type of substrate used in casting methods significantly influences the surface roughness and morphology of the resulting films. Different substrates, such as smooth glass and patterned Teflon®, lead to distinct optical and structural properties, affecting a film's final characteristics. Films cast on smooth substrates, such as borosilicate glass, exhibit higher transparency and uniformity, while those cast on rough substrates, like Teflon®, develop increased surface roughness due to micro-patterning during drying [37]. Studies indicate that the roughness exponent and growth exponent vary depending on the substrate type, with rough surfaces leading to a reduction in growth exponent during the initial deposition phases [38].

On smooth substrates, nanoparticles in films tend to align in layers along the growth direction—a phenomenon that becomes less prominent with increasing substrate roughness [39]. The evolution of film morphology follows specific scaling laws, indicating that substrate roughness significantly impacts the dynamic evolution of surface features [40]. While substrate type is a critical factor, other parameters, such as humidity, must also be considered, as they further influence film properties, suggesting a complex interplay of variables in film production.

Despite these advances, the role of the casting substrate as a key factor influencing starch film structure and properties has not been fully addressed. In this study, we present a novel approach by maintaining a fixed starch–glycerol composition and evaluating how different casting substrates—glass, acrylic, and PTFE—influence film roughness, surface energy, mechanical strength, and optical behavior.

The novelty of this work lies in isolating the substrate variable while keeping film composition constant, providing clear insight into how manufacturing methods influence biodegradable films' functionality. Such understanding is essential for scaling up biodegradable packaging technologies, wherein substrate choice may be limited by industrial processing methods.

## 2. Materials and Methods

Four different substrates were prepared to investigate the effect of the surface on the resulting film.

- Glass—a glass bed from a Zmorph S.A. Wrocław, Poland;

A glass 3D-printing bed is characterized by its exceptionally low roughness, smooth surface, and high adhesion properties, which are essential for maintaining print stability during fused deposition modeling (FDM).

- Laminate—a laminate plate (without copper) manufactured by Aksotrnik spółka z ograniczoną odpowiedzialnością, Nowy Konik, Poland

Glass–epoxy composites exhibit a slightly higher surface roughness compared to a glass printing bed while maintaining a similarly smooth surface and strong adhesion properties.

- Copper—a glass–epoxy laminate with copper on one side, manufactured by OEM

The copper surface exhibits subtle, barely perceptible patterns, indicating a macroscopically non-ideal smoothness. However, these patterns are not tactilely discernible.

- Teflon®—a PTFE plate

The Teflon surface used in this study is a standard laboratory component, exhibiting surface scratches likely resulting from routine usage. Additionally, the surface is characterized by its inherent low adhesion properties, which contribute to its wide range of applications.

A solution of food-grade potato starch, vegetable glycerin, and water was prepared in the following concentrations:

Starch—5% by weight;
Glycerine—2% by weight;
Water—93% by weight.

The prepared mixture was heated with continuous stirring until a homogeneous solution was obtained. The temperature was increased to approximately 90 degrees Celsius. The resulting solution was then allowed to cool to a temperature between 50 and 60 degrees Celsius, after which it was poured onto the prepared materials and spread using a doctor blade. To ensure a uniform initial solution thickness of 3 mm, the films were cast using an Micrometer Adjustable Film Applicator from RK Print Coat Instruments, Litlington, UK. The coated plates were left to dry at room temperature. After 10 days of drying, the plates were removed and subjected to static peel testing.

Tensile testing was conducted in accordance with ISO 527-3 standard [41]. The following parameters were maintained:

- Sample Width, $15 \pm 0.2$ mm;
- Sample Length, 50 mm;
- Tensile Speed, $100 \pm 10$ mm/min.

The mechanical properties of the fabricated films were evaluated using a Zwick-Roell Z010 tensile testing machine (ZwickRoell, Ulm, Germany) equipped with a 1 kN load cell. Ten replicates were tested for each sample, and the average value was reported as the final result.

The surface tension and wettability of both the starch film-forming solutions and the resulting starch films were investigated. Water contact angle (WCA) measurements were performed according to ISO 15989 [42] using a Drop Shape Analysis System (DSA 30E, Krüss, Hamburg, Germany). The surface free energy was calculated using the Owens–

Wendt–Rabel–Kaelble (OWRK) method [43] based on static contact angle measurements with water and diiodomethane.

For the measurements, films were cut into approximately 2.5 cm × 6 cm rectangular specimens. Sessile drops of water and diiodomethane were dispensed onto the film surface using needles with a 0.5 mm diameter. The static contact angle was determined using the Tangent 2 method, measured 5 s after droplet deposition.

The surface morphologies of the samples were examined using a Keyence VHX-950F digital optical microscope equipped with a VH-Z100R zoom lens (100–1000× magnification) (Keyence Corp., Itasca, IL, USA). In addition to acquiring standard micrographs of the sample surfaces, three-dimensional surface topography reconstruction was performed. This was achieved by capturing a series of images at varying focal planes, enabling the determination of surface roughness. Photographs of cross-sections of the samples were also taken. The material was sectioned using a punch and press.

In addition, to gain more insight into the surface morphology, electron mapping was carried out using SEM (JOEL JCM-7000, JEOL USA Inc., Peabody, MA, USA) with an acceleration voltage of 15 kV. Before SEM analyses, the samples were covered with a thin gold layer.

The water vapor transmission rate (WVTR) of the films was determined, as it is a critical parameter for packaging applications. WVTR measurements were conducted using a Radwag MA 210.R moisture analyzer (Radwag, Radom, Poland) equipped with a dedicated WVTR vessel. Circular film samples with a diameter of 54 ± 2 mm were prepared. Each sample was placed on an aluminum-sealed vessel containing 5 g of distilled water and then inserted into the analyzer's test chamber. The chamber temperature was maintained at 40 °C, while the ambient conditions were kept at 23 ± 0.5 °C and 50 ± 1% relative humidity (RH).

The mass of the water within the vessel was recorded manually at 0, 1, and 2 h intervals. The WVTR was calculated using the following equation:

$$\mathrm{WVTR} = \frac{m_1 - m_2}{t \cdot S} \quad (1)$$

The notation above is described below:

- $m_1$ and $m_2$ represent the mass of water (g) after 1 and 2 h, respectively;
- $t$ is the time interval (1 h);
- $S$ is the surface area of the film sample ($m^2$).

Water vapor permeability was measured due to its critical importance in the packaging industry, a major sector exploring the application of biodegradable materials. Understanding the rate at which water vapor permeates packaging is essential for determining the suitability of these materials for food product packaging.

Film colorimetric properties were assessed using an X-Rite eXact spectrophotometer (X-Rite Inc., Grand Rapids, MI, USA) under standardized conditions: D50 illuminant, 2° standard observer, and M0 measurement mode. To comprehensively characterize the films' color behavior, measurements were conducted over both white and black backing substrates. These substrates were selected for their near-ideal light reflectance and absorption properties, respectively. Baseline measurements were taken for the substrates alone, and subsequent measurements were performed with the films applied. Colorimetric changes induced by the films were then calculated by comparing the measurements with and without the films present.

## 3. Results

### 3.1. Process for Obtaining Samples

The initial step in sample preparation involved the creation of a homogeneous mixture. A glass beaker was placed on an analytical balance, and potato starch, glycerol, and deionized water were sequentially added. The mass of each component was measured with an accuracy of 0.02 g. Following the preparation of the solution, a magnetic stir bar was introduced, and the beaker was positioned on a hot plate with magnetic stirring capabilities. A thermometer was immersed in the mixture, initiating a controlled heating and stirring process.

The temperature was gradually increased to a range of 80–90 °C. At approximately 70–80 °C, an increase in both the transparency and viscosity of the mixture was observed, originating from the heat source. Subsequently, the rate of temperature increase slowed. Prior to this point, the temperature had been rising between 5 and 10 degrees per minute, at which point the rise slowed to about two degrees per minute. Shortly thereafter, a decrease in the mixture's viscosity occurred, although it did not return to its initial value. Once the entire mixture had undergone these transformations, it was removed from the heat source and allowed to cool partially, facilitating the subsequent pouring process.

#### 3.1.1. Pouring of the Film

During the casting process, Teflon exhibited distinct behavior compared to the other materials. The application of the hot solution (50–60 °C) induced significant thermal shrinkage, leading to challenges in achieving a uniform material distribution. In contrast, all the other materials tested exhibited no noticeable reactions or dimensional changes under the same conditions.

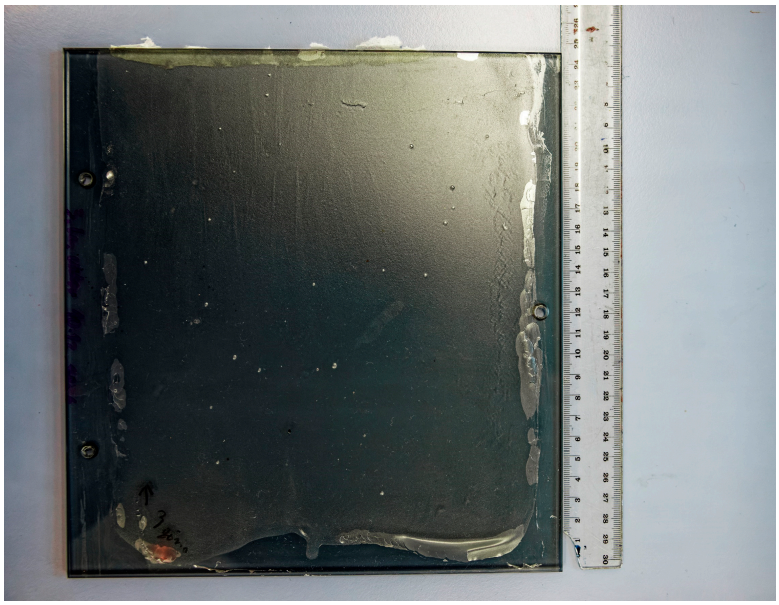
#### 3.1.2. Film Removal

As anticipated, the potato starch films exhibited varying degrees of adhesion to different substrate surfaces. This variability in adhesive strength is likely due to differences in surface energy, roughness, and chemical compatibility between the starch film and the respective substrates.

The potato starch films demonstrated strong adhesion to glass substrates, requiring careful removal to obtain intact sheets for subsequent tensile testing. Despite the robust adhesion, complete film sheets were successfully detached. However, localized areas of thinner regions of the film were observed along the edges, resulting in partial detachment from the glass substrate. These edge defects are visually documented in Figure 1.

The potato starch films displayed an adhesion pattern on copper-free laminate substrates similar to that observed on glass. A significant adhesive force was present, yet it did not impede the detachment of complete film sheets. Similar to the glass substrates, natural detachments were observed, and the intact film sheets, along with the removal process, are illustrated in Figure 2. Notably, the areas where the film naturally detached from the laminate surface due to drying did not exhibit the cracking observed on the glass substrates.

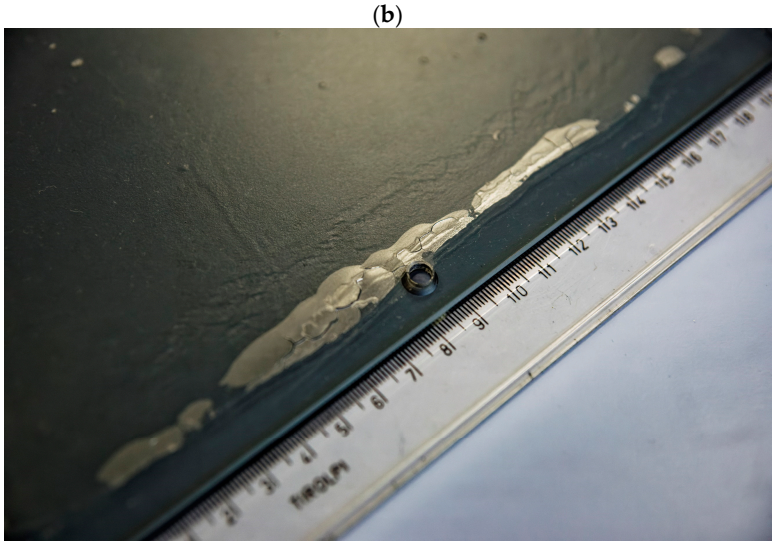
Copper substrates exhibited the strongest adhesion to the cast potato starch films. The adhesive forces exceeded the cohesive forces within the film, resulting in film rupture during attempts to detach it from the copper surface. As a result, obtaining an intact film sheet for static tensile testing was impossible. The morphology of the cast material and the observed natural detachments are depicted in Figure 3.



(**a**)

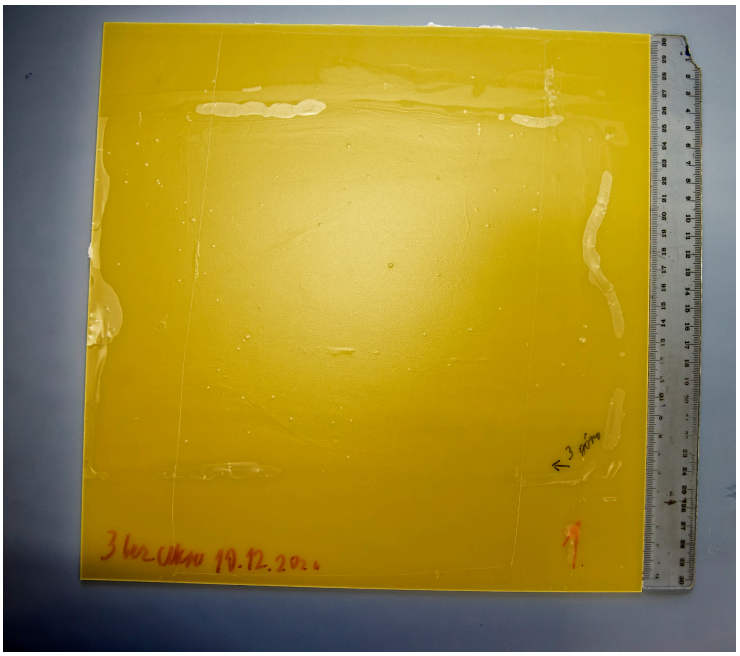


(**b**)

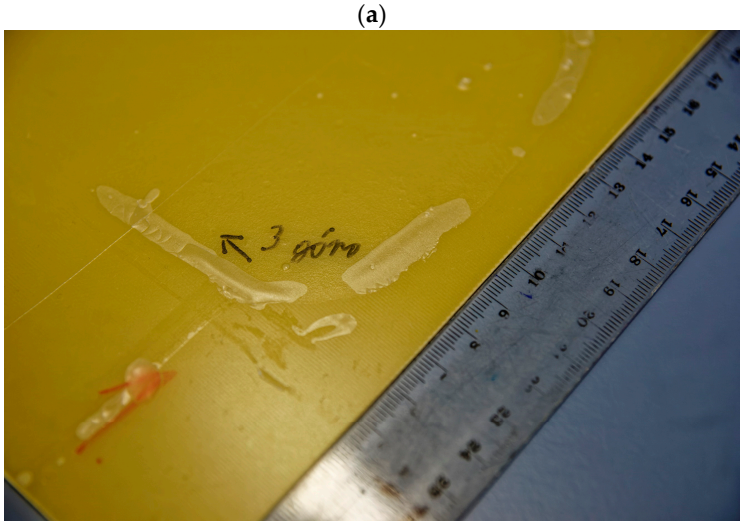


(**c**)

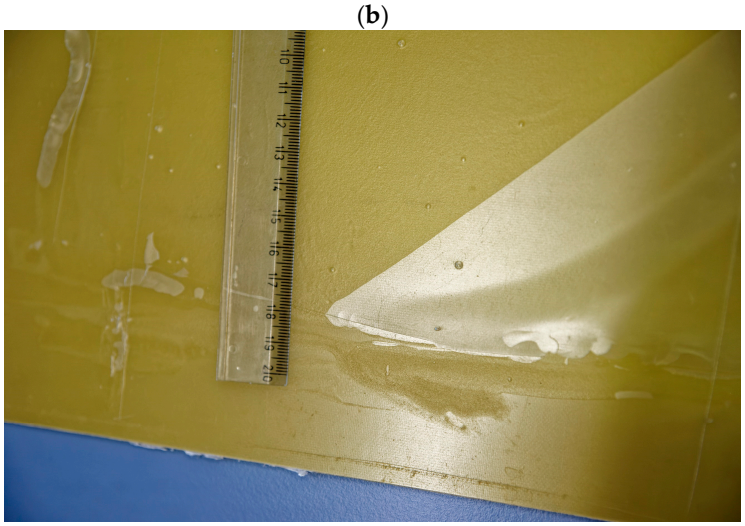
**Figure 1.** Photographs showing all of the poured films (**a**) and where the films naturally detach from the substrate as a result of the drying process (**b**,**c**).



(**a**)



(**b**)



(**c**)

**Figure 2.** Photographs showing all of the poured films on the surface of the copper-free laminate (**a**), the areas where natural peeling from the surface occurred (**b**), and the partially peeled film (**c**).



(**a**)



(**b**)

**Figure 3.** The copper plates (**a**) on which the film was poured are shown, as well as the areas where the foil was observed to naturally detach from the substrate (**b**).

In contrast, Teflon® substrates demonstrated the weakest adhesion, detaching spontaneously from the surface. However, the resulting film material displayed increased waviness.

### *3.2. Tensile Testing*

The results regarding mechanical properties are summarized in Table 1. The results indicate a potential advantage of the films deposited on glass surfaces, both in terms of the pressure required for rupture and the percentage elongation. However, considering measurement uncertainty, these differences are not statistically significant, preventing a definitive conclusion. Nevertheless, this does not exclude the possibility of such a relationship.

**Table 1.** Results of tensile testing of samples dried on various surfaces.

| Substrate | Tensile Strength (MPa) | ± | Elongation at Break (%) | ± |
|---|---|---|---|---|
| Laminate | 4.93 | 0.391 | 88 | 15 |
| Glass | 5.62 | 0.492 | 93 | 26 |
| Teflon® | 4.69 | 0.74 | 62 | 16 |

The films cast on Teflon exhibited statistically significantly less elongation. This may be attributed to the drying process, which appeared more irregular as the film detached from the surface, as previously described.

Furthermore, it is worth highlighting that the samples produced on copper-free laminate exhibited the lowest measurement uncertainty and the highest repeatability.

### 3.3. Surface Free Energy

Table 2 shows the results of surface free energy, SFE, and its dispersive and polar components measured on the starch films' top or bottom surface and the substrate surface used for film development.

**Table 2.** The values of SFE together with its dispersion and polar component.

| Surface | Dispersion Component [mJ·m$^{-2}$] | Polar Component [mJ·m$^{-2}$] | Surface Free Energy [mJ·m$^{-2}$] |
|---|---|---|---|
| Glass—top | 42.01 | 31.59 | 73.60 |
| Glass—bottom | 44.77 | 26.95 | 71.71 |
| Glass—material | 40.88 | 22.90 | 63.78 |
| Laminate—top | 43.03 | 27.62 | 70.66 |
| Laminate—bottom | 42.89 | 29.54 | 72.44 |
| Laminate—material | 35.77 | 19.93 | 55.69 |
| Copper—top | 38.20 | 9.63 | 47.83 |
| Copper—bottom | 34.68 | 0.53 | 35.21 |
| Copper—material | 38.20 | 9.63 | 47.83 |
| Teflon®—top | 39.72 | 28.08 | 67.80 |
| Teflon®—bottom | 37.15 | 10.55 | 47.70 |

The SFE analysis demonstrated a significant influence of substrate type on the surface characteristics of the resulting films. A nonlinear relationship was observed between the substrate material and the SFE value. The films cast on glass and laminate exhibited similar SFE values, approximately 70 mJ·m$^{-2}$, whereas the substrates themselves showed values of 64 and 56 mJ·m$^{-2}$, respectively.

In contrast, the films cast on copper showed significantly lower SFE values, measuring 48 mJ·m$^{-2}$ (top side), 35 mJ·m$^{-2}$ (bottom side), and 48 mJ·m$^{-2}$ (bulk material). These results indicate that the substrate type affects not only the bottom layer of the film but also its top surface. This finding has significant implications for the potential applications of the films, such as printing, where a high SFE value is desirable. A higher SFE improves the wetting of a film's surface by ink, as the surface tension of the ink must be lower than the SFE of the substrate to ensure proper adhesion.

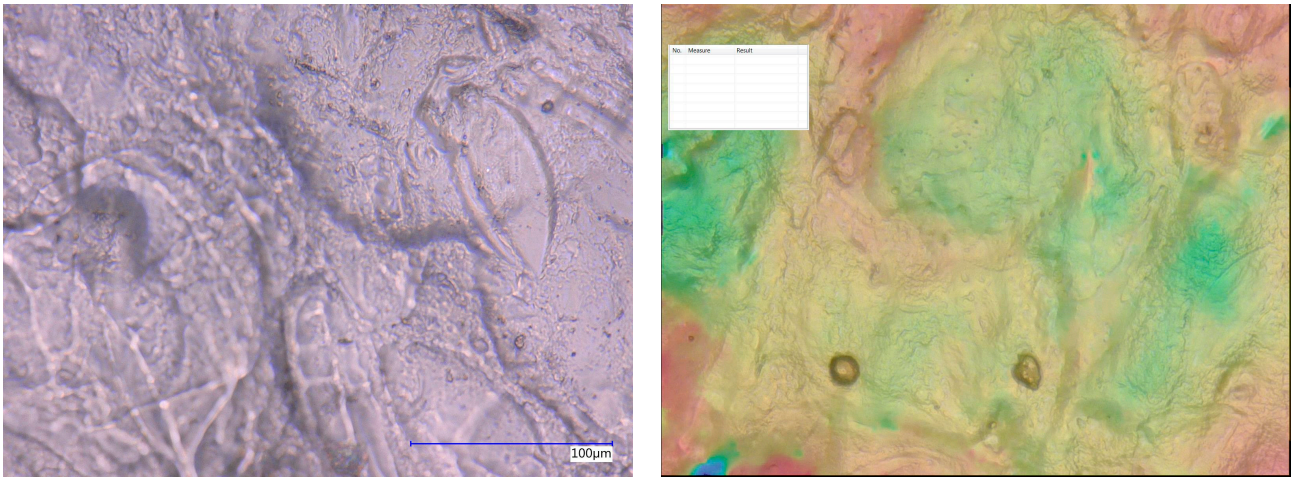
### 3.4. Microscopic Images

Each sample was excised from a sheet and subjected to microscopic examination. Micrographs were acquired at progressively increasing magnifications at the same sample location, using magnification levels of 100×, 200×, 500×, and 1000×. Subsequently, a series of images was captured to reconstruct the three-dimensional surface and analyze its roughness. Images of the top layer are presented first, followed by those of the bottom layer. Where applicable, a height map overlay is included alongside the corresponding micrograph.

#### 3.4.1. Glass

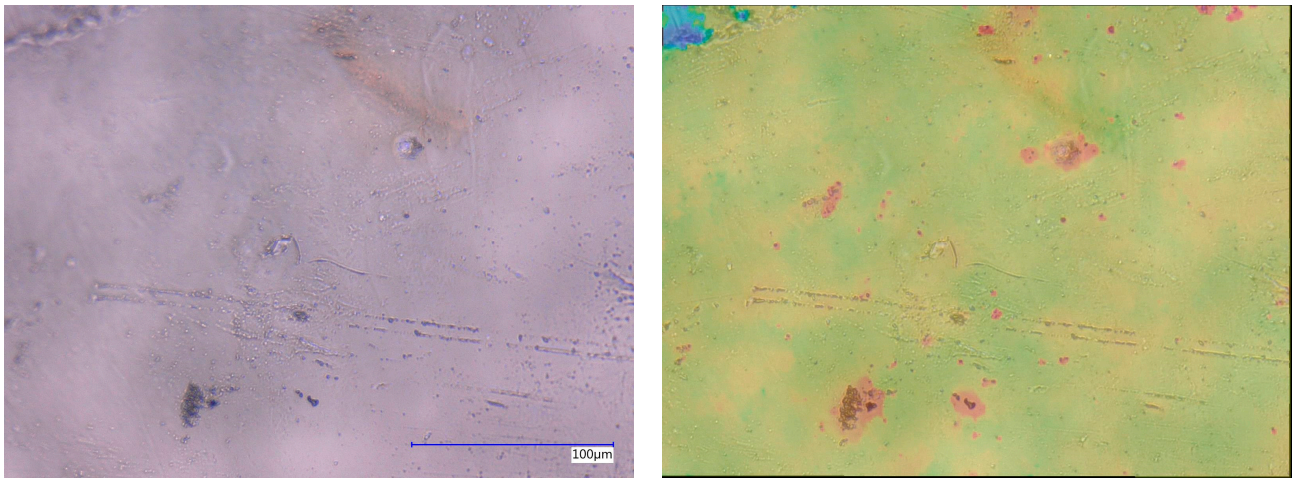
The micrographs of the top surface, presented in Figure 4 and Appendix A.1, reveal a corrugated and irregular morphology consistent with the expected structure of a

starch-based film. In contrast, the bottom-surface micrographs, shown in Figure 5 and Appendix A.2, exhibit a significantly more intriguing texture. At 1000× magnification, it is evident that the majority of the surface is remarkably transparent, allowing clear visualization of the film's reverse side. Only a few irregularities are apparent, including structures resembling microscratches and small formations of a dark, slightly reflective material.




(**a**) (**b**)

**Figure 4.** Microscopic images of the top layer of the film obtained on a glass surface at 1000× magnification (**a**) and an elevation map (**b**), red indicates the highest points, blue the lowest.

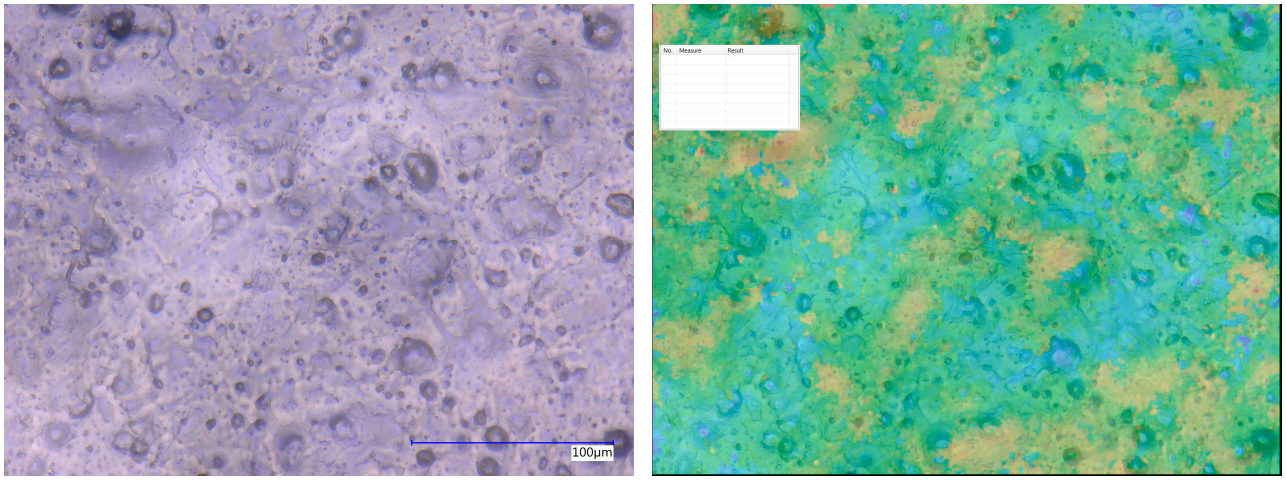



(**a**) (**b**)

**Figure 5.** Microscopic images of the bottom layer of the film obtained on a glass surface with optical zoom of 1000 (**a**) and an elevation map (**b**), red indicates the highest points, blue the lowest.

### 3.4.2. Laminate

The top-surface micrographs of the film deposited on the laminate do not reveal any distinctive features, as presented in Figure 4, displaying only disordered structures (more are shown in Appendix A.3). The micrographs of the bottom surface, depicted in Figure 6 and Appendix A.4, exhibit a higher degree of structural organization, although further conclusive interpretation is challenging.

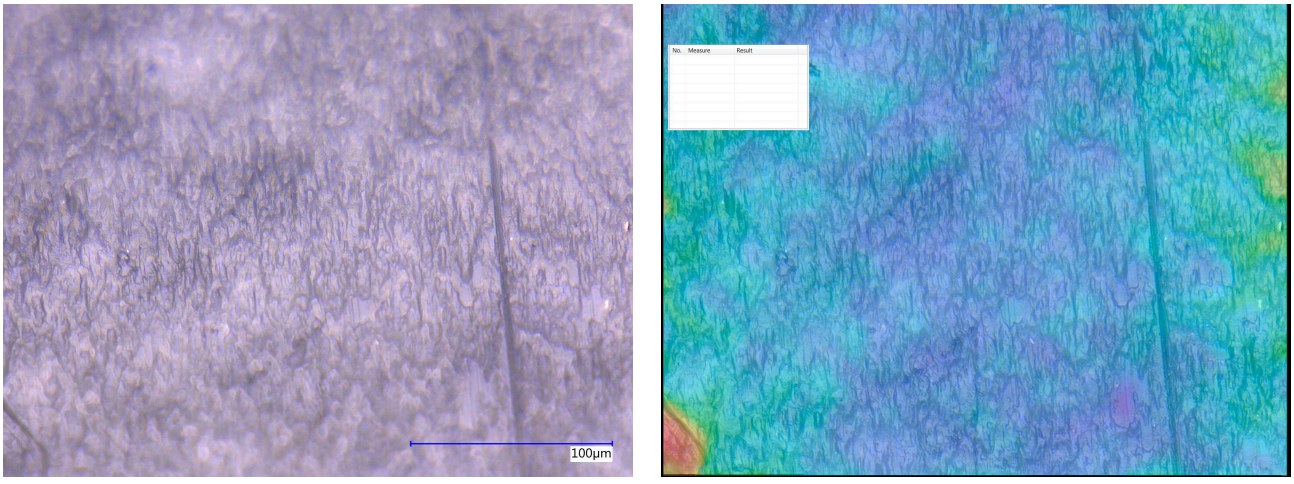



(**a**) (**b**)

**Figure 6.** Microscopic images of the bottom film layer obtained on the laminate surface with optical zoom level of 1000 (**a**) and an elevation map (**b**), red indicates the highest points, blue the lowest.

### 3.4.3. Copper

The top surface of the material deposited on copper exhibits no notable deviations, presenting solely disordered structures (shown in Appendix A.5). In contrast, the bottom surface, depicted in Figure 7 and Appendix A.6, reveals distinct, unidirectionally aligned striations. These striations range in width from several micrometers, with lengths spanning tens to hundreds of micrometers. This observation may explain the high adhesion to the copper substrate and the challenges encountered during film detachment. Notably, the three-dimensional surface reconstruction failed to accurately replicate these microstriations, potentially affecting roughness analysis.

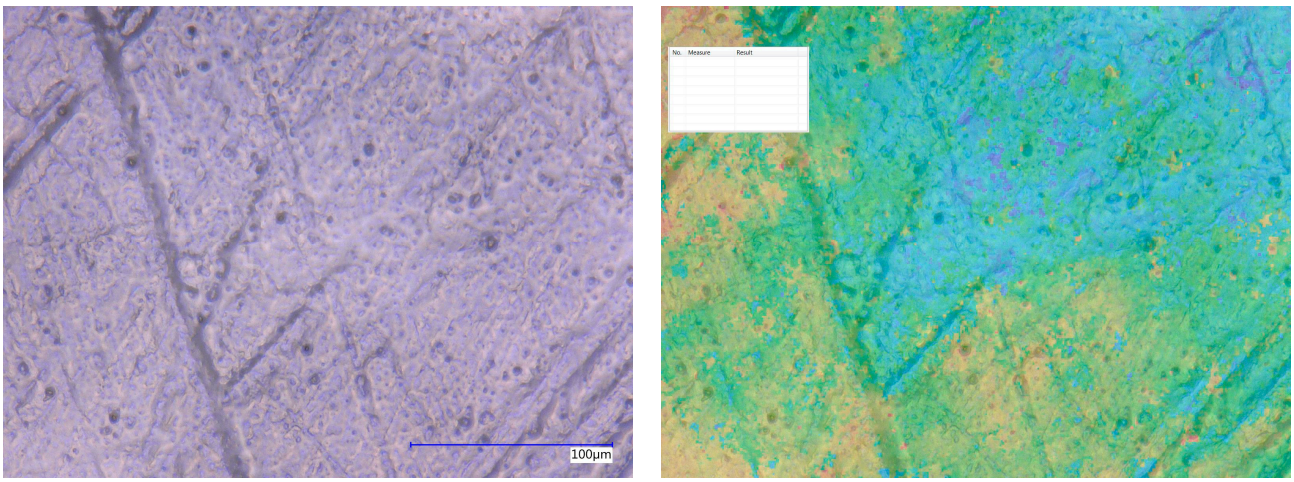



(**a**) (**b**)

**Figure 7.** Microscopic images of the bottom film layer obtained on the copper surface with optical zoom level of 1000 (**a**) and an elevation map (**b**), red indicates the highest points, blue the lowest.

### 3.4.4. Teflon

Similarly, the top surface of the film deposited on Teflon® did not exhibit any unexpected morphological features (depicted in Appendix A.7). However, the bottom surface, shown in Figure 8 and Appendix A.8, reveals distinct substrate imperfections, appearing as if scratches from the Teflon surface were imprinted onto the material during the drying process.




(**a**) (**b**)

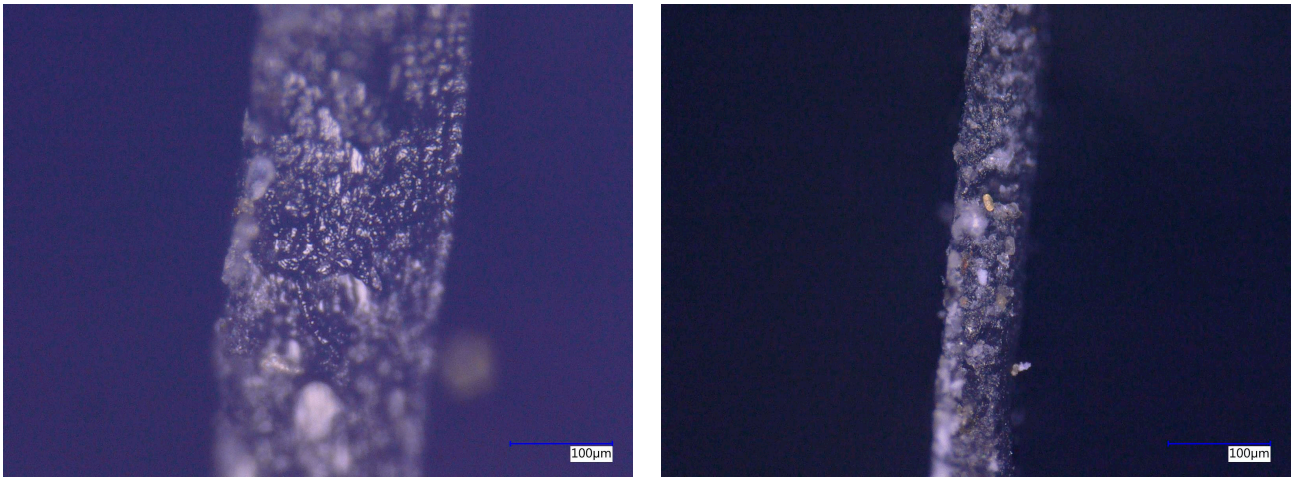
**Figure 8.** Microscopic images of the bottom film layer obtained on the Teflon® surface with an optical zoom of 1000 (**a**) and an elevation map (**b**), red indicates the highest points, blue the lowest.

Alongside standard surface optical images, cross-sectional optical images of the cut material are included. When analyzing these images, it is crucial to consider that the cutting technique itself may have introduced artifacts into the resulting cross-section.

3.4.5. Cross-Section

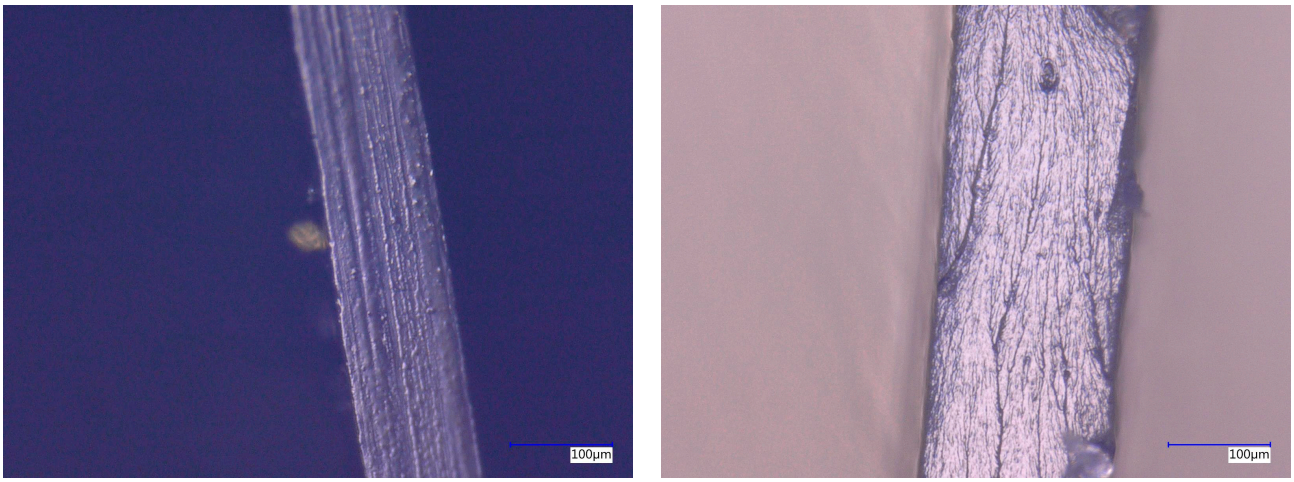
The cross-sectional morphology of the glass film (Figure 9a) exhibits a crystalline or lithic appearance. The surface presents a rough texture, with observable orange-rust-colored inclusions. These inclusions are potentially attributable to contamination from the cutting instrument used to prepare the cross-section. Furthermore, the film demonstrates non-uniform thickness at both lower (a) and higher (b) magnifications.

The cross-sectional analysis of the laminate (Figure 9b) reveals a pronouncedly irregular surface morphology. Furthermore, the presence of orange-copper particulate matter can be observed, potentially indicating contamination from the cutting instrument. Alternatively, this observation may correlate with uncharacterized material properties. Future investigations are warranted to elucidate the origin of these findings.




(**a**) (**b**)

**Figure 9.** *Cont.*




(**c**) (**d**)

**Figure 9.** The figure shows a cross-section at 500 times magnification of a film made on glass (**a**), laminate (**b**), copper (**c**) and Teflon (**d**).

The cross-sectional analysis of the copper-cast foil (Figure 9c) reveals a uniformly smooth surface morphology. Several factors may contribute to this observation. Firstly, the substrate upon which the foil was sectioned likely facilitated a more regular cut. Secondly, the robust adhesion between the deposited material and the wafer substrate may have mitigated irregularities during the film desiccation process. Furthermore, the potential influence of a controlled electrical field during fabrication cannot be discounted. Consequently, the observed cross-sectional structure presents a compelling subject for further investigation to elucidate its formation mechanism.

The cross-sectional analysis of the film cast on Teflon (Figure 9d) revealed a reticulated structure, reminiscent of leaf venation. A wider field of view reveals discontinuities along the edge, likely attributable to fragment detachment during sectioning. We hypothesize that this structure is a consequence of the desiccation process, which is more stochastic on Teflon due to diminished surface adhesion. These findings are of significant interest.

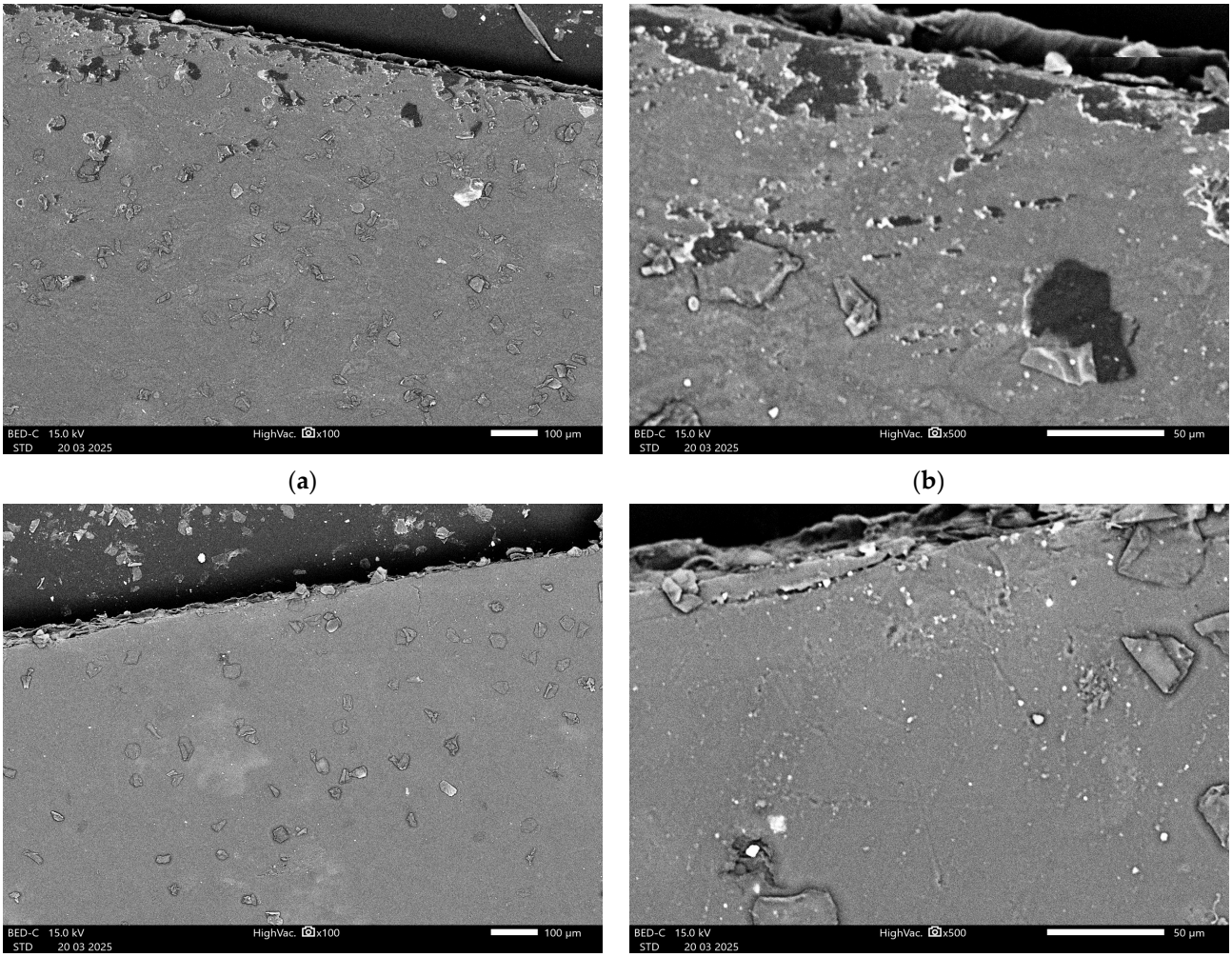
### *3.5. SEM*

#### 3.5.1. Glass

Scanning electron microscopy (SEM) analysis of the surface of the film deposited on glass (Figure 10) revealed a predominantly uniform morphology, punctuated by localized speckles and irregular deposits near the periphery. These deposits are particularly prominent on the top layer at higher magnification (b). Conversely, the bottom surface exhibits a significantly smoother texture (c, d). While the top surface generally maintains regularity, the aforementioned peripheral deposits are still observable (a).

#### 3.5.2. Laminate

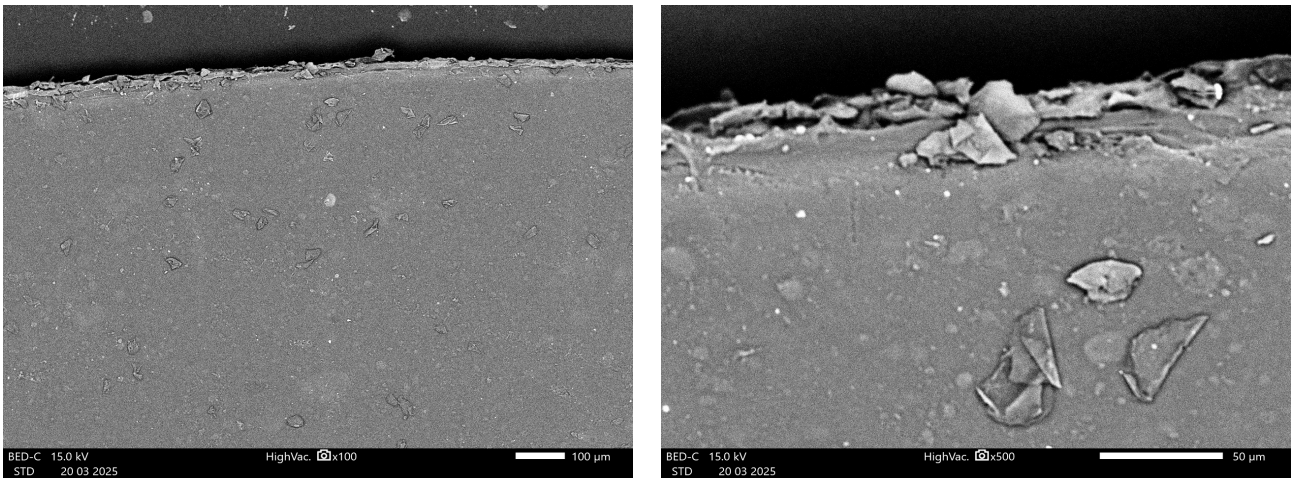
The scanning electron microscopy (SEM) images presented in Figure 11, depicting the surface of the film deposited on the laminate, reveal a high degree of uniformity. Both the lower and upper (a) surfaces exhibit minimal irregularities, with the exception of pollen-like particulates.




(**a**) (**b**)

(**c**) (**d**)

**Figure 10.** Scanning electron microscopy (SEM) images of a film cast on glass are presented, showcasing the top layer at magnifications of 100× (**a**) and 500× (**b**) and the bottom layer at magnifications of 100× (**c**) and 500× (**d**).

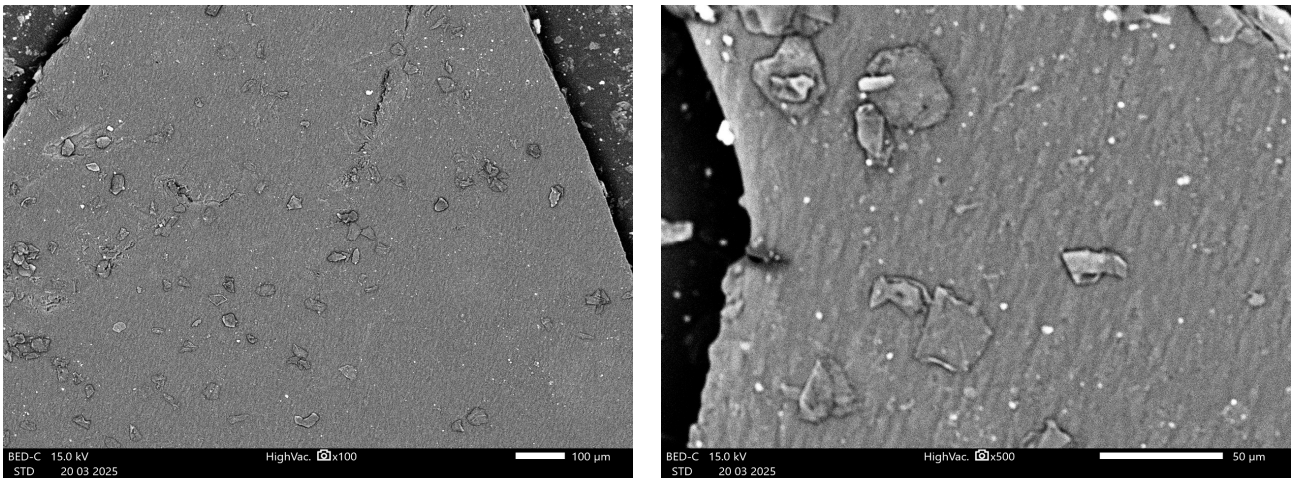



(**a**) (**b**)

**Figure 11.** Scanning electron microscopy (SEM) images of a film cast on laminate are presented, showcasing the bottom layer at magnifications of 100× (**a**) and 500× (**b**).

### 3.5.3. Copper

The images presented in Figure 12 reveal certain surface irregularities. Specifically, the lower layer (a, b) exhibits punctate features, which were also shown in the optical micrographs.

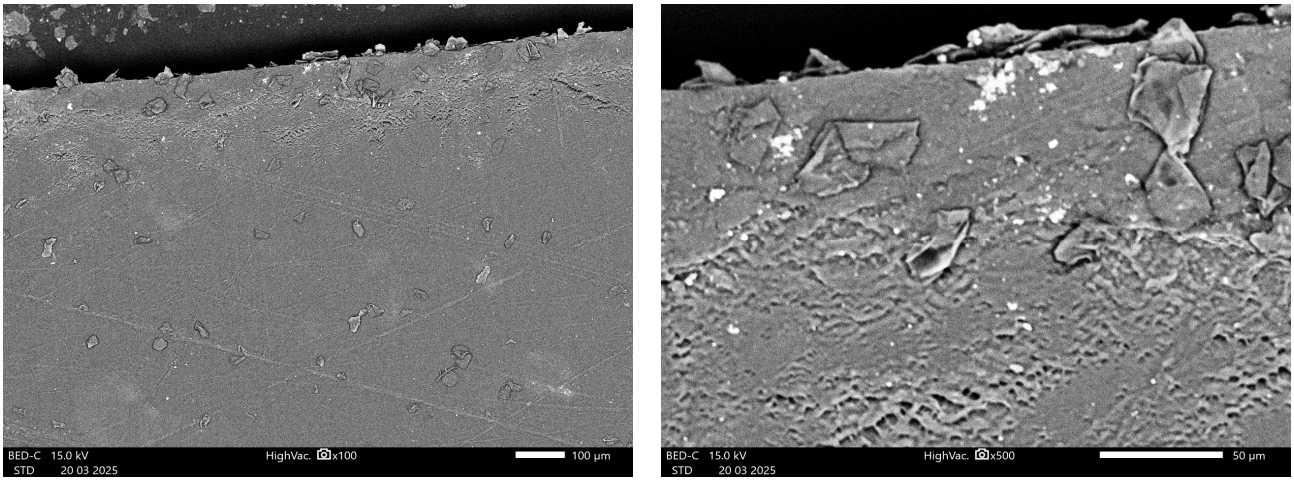



(**a**) (**b**)

**Figure 12.** Scanning electron microscopy (SEM) images of a film cast on copper are presented, showcasing the bottom layer at magnifications of 100× (**a**) and 500× (**b**).

### 3.5.4. Teflon

The micrographs of the film cast on Teflon (Figure 13) reveal intriguing surface characteristics. The irregularities present on the upper layer are reminiscent of those seen on the other film samples (shown in Appendix A.11). However, the lower layer exhibits distinct linear striations (a), which correlate with the optical microscopy observations. Furthermore, a unique textured morphology is evident (b), where the features align with the aforementioned striations but present a significantly rougher surface topology.




(**a**) (**b**)

**Figure 13.** Scanning electron microscopy (SEM) images of a film cast on Teflon are presented, showcasing the bottom layer at magnifications of 100× (**a**) and 500× (**b**).

## *3.6. Roughness*

The basic surface roughness parameters are listed in Table 3.

**Table 3.** Surface roughness measurement results for starch films.

| | Sa [µm] [1] | Sz [µm] [2] | Sq [µm] [3] | Ssk [4] | Sku [5] | Sp [µm] [6] | Sv [µm] [7] |
|---|---|---|---|---|---|---|---|
| Glass—top | 1.88 | 13.04 | 2.30 | 0.05 | 2.34 | 5.86 | 7.18 |
| Glass—bottom | 0.14 | 3.20 | 0.18 | 1.63 | 17.86 | 2.68 | 0.52 |
| Laminate—top | 0.92 | 7.23 | 1.13 | 0.19 | 2.67 | 3.74 | 3.49 |
| Laminate—bottom | 0.57 | 9.95 | 0.76 | 0.18 | 5.02 | 4.69 | 5.26 |
| Copper—top | 1.89 | 13.89 | 2.29 | 0.47 | 2.76 | 7.79 | 6.10 |
| Copper—bottom | 0.30 | 2.38 | 0.38 | 0.43 | 2.89 | 1.33 | 1.05 |
| Teflon®—top | 1.47 | 10.45 | 1.84 | 0.60 | 3.21 | 6.12 | 4.33 |
| Teflon®—bottom | 0.96 | 11.98 | 1.21 | 0.28 | 3.56 | 5.87 | 6.11 |

[1] Sa (arithmetic mean height): the average absolute deviation of the surface from the mean plane. [2] Sz (maximum height): the vertical distance between the highest peak and the lowest valley within the measured area. [3] Sq (root mean square height): the root mean square (RMS) average of the height deviations from the mean plane. [4] Ssk (skewness): indicates the asymmetry of the height distribution. A positive value suggests a surface with more peaks than valleys. [5] Sku (Kurtosis): describes the sharpness of the height distribution. A value close to 3 indicates a Gaussian distribution. [6] Sp (maximum peak height): the height of the tallest peak above the mean plane. [7] Sv (maximum valley depth): the depth of the deepest valley below the mean plane.

The results of the top surface roughness measurements show similar values for copper and glass. The Teflon® surface exhibited slightly higher roughness, whereas the laminate surface demonstrated roughness values approximately twice as high as those of copper and glass.

In contrast, there were varying results regarding the roughness of the bottom layer in contact with the surface for each of the materials tested. The highest roughness was recorded for Teflon® (0.96 µm), followed by laminate (0.57 µm) and copper (0.30 µm). The lowest roughness was observed for glass (0.14 µm).

It is important to acknowledge that three-dimensional surface reconstruction has inherent limitations; therefore, certain results may deviate from the true surface characteristics.

### *3.7. Water Vapor Permeability*

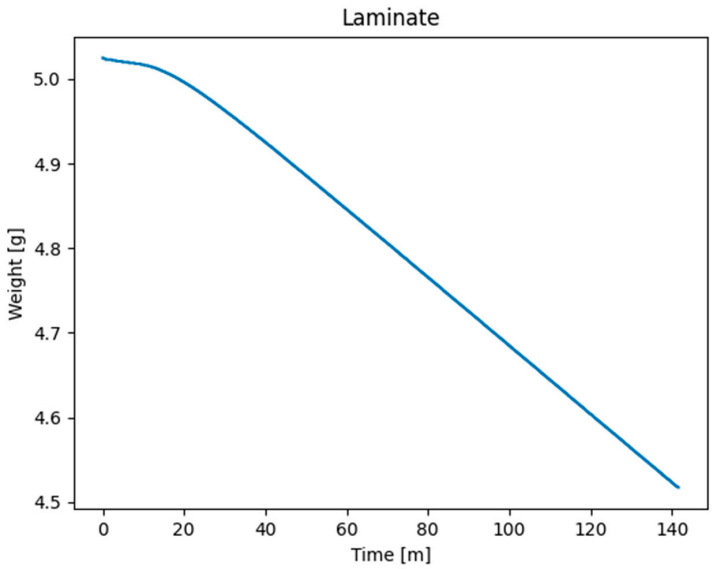
The test was conducted at 40 degrees Celsius. Each sample was subjected to at least two 60 min measurement cycles. Control values were recorded after 1 and after 2 h.

The results of the vapor permeability tests (Table 4) indicate that surface properties have no significant effect on this parameter. The observed water vapor flux, oscillating around $4 \times 10^{-4}$ kg/m$^2$s for all the films tested, suggests that the material has low vapor permeability.

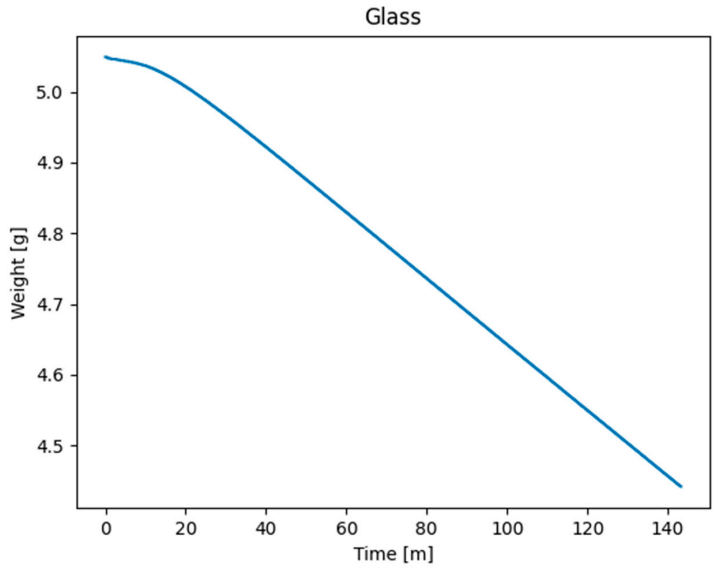
**Table 4.** Water vapor permeability measurement results.

| Substrate | $m_1$ [g] | $m_2$ [g] | $\Delta m$ [g] | WVTR [kg·m$^{-2}$·s$^{-1}$] | WVTR [kg·m$^{-2}$·day$^{-1}$] |
|---|---|---|---|---|---|
| Glass | 4.829 | 4.55 | 0.279 | 0.000337 | 29.113043 |
| Laminate | 4.846 | 4.604 | 0.242 | 0.000292 | 25.252173 |
| Teflon | 4.890 | 4.669 | 0.221 | 0.000267 | 23.060869 |

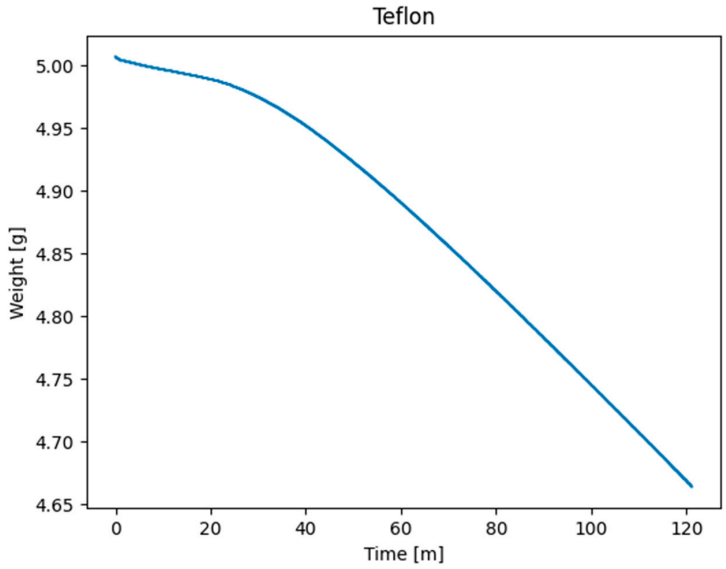
The mass change plots, depicted in Figure 14, do not exhibit any anomalous behaviors. An initial rate of change within the first hour can be observed, likely due to thermodynamic fluctuations and the saturation of the material with water vapor. The process stabilizes after 30 to 40 min.




(**a**)




(**b**)




(**c**)

**Figure 14.** Graph of water mass changes over time for laminate (**a**), glass (**b**), and Teflon® (**c**).

### 3.8. Color

To precisely evaluate the colorimetric properties of the films obtained, measurements were performed using substrates with contrasting optical properties—white and black. This methodology enabled a comprehensive analysis of the effect of a film's transparency on its perceived color while minimizing potential artifacts resulting from the interaction of light with a single type of substrate. The values of the color parameters $L$, $a$, $b$ with $\Delta L$, $\Delta a$ $\Delta b$ and total color difference $\Delta Lab$ are shown in Table 5. The color difference $\Delta L$, $\Delta a$ $\Delta b$ was calculated as the difference between the measurement of the film on the substrate and the substrate itself. The total color difference was determined according to the Equation (2):

$$\Delta Lab = \sqrt{(\Delta L)^2 + (\Delta a)^2 + (\Delta b)^2} \quad (2)$$

**Table 5.** $L$, $a$, $b$ color parameters together with $\Delta L$, $\Delta a$ $\Delta b$ and total color difference $\Delta Lab$ for the starch films developed.

| Substrate | Measuring Base | $L$ | $a$ | $b$ | $\Delta L$ | $\Delta a$ | $\Delta b$ | $\Delta Lab$ |
|---|---|---|---|---|---|---|---|---|
| Copper | Black | 32.67 | −0.48 | −1.15 | −22.47 | 0.9 | 1.48 | 22.53666568 |
| | White | 100.84 | 0.76 | −5.58 | 2.58 | 0.38 | −1.6 | 3.059542449 |
| Glass | Black | 28.87 | −0.13 | −0.75 | −18.67 | 0.55 | 1.08 | 18.70929715 |
| | White | 100.87 | 0.88 | −6.54 | 2.55 | 0.26 | −0.64 | 2.641912186 |
| Laminate | Black | 27.18 | 0.03 | −0.05 | −16.98 | 0.39 | 0.38 | 16.98872862 |
| | White | 100.84 | 0.85 | −6.43 | 2.58 | 0.29 | −0.75 | 2.702406335 |

Colorimetric analysis of the films revealed distinct color changes, with a predominant white hue. Changes in $\Delta Lab$ values below 3 units are generally considered visually indistinguishable. In this study, $\Delta Lab$ values within this range were measured on a white substrate. Conversely, significant $\Delta Lab$ changes, ranging from 17 to 22 units, were observed on a black substrate; these changes were readily perceptible to the naked eye. Furthermore, the results indicate a substrate-dependent influence on film color. The most pronounced $\Delta Lab$ changes, on both white and black substrates, were observed for the films cast on copper. However, further studies should be conducted to strengthen the statistical evidence and exclude potential confounding factors. These color variations may be attributed to material aging, solar exposure during drying, and doctor blade parameters during the film formation process.

## 4. Discussion

The results of this study unequivocally demonstrate that substrate type significantly influences the properties of the resulting starch-based films despite the laboratory-scale nature of the casting method, which limits direct scalability to industrial production. Nevertheless, the identification of the substrate's influence on film properties is crucial for optimizing the formulation and manufacturing conditions for mass production.

The observations regarding the difficulty of removing the films from copper substrates and the damage to the films cast on Teflon® highlight the critical role of interfacial adhesion. Optimal results were achieved for the laminate and glass substrates, suggesting that these materials provide a favorable balance between adhesion and ease of separation.

Mechanical property analysis did not reveal statistically significant differences in tensile strength across the various substrates. However, the lower elongation values observed for the films cast on Teflon suggest a possible influence of drying conditions on mechanical properties. This does not preclude potential influences of the substrate on other aspects of mechanical performance, a topic beyond the scope of this study. Existing

studies report varying tensile strength properties for these materials, with some indicating values of around 5 MPa at the point of rupture, while others suggest values closer to 10 MPa [44]. This discrepancy may be attributed to variations in sample moisture content and compositional differences.

The surface free energy (SFE) analysis revealed a non-linear correlation between substrate material and the resulting film surface characteristics. Specifically, the films deposited on glass and laminate exhibited comparable SFE values, approximating 70 $mJ \cdot m^{-2}$, despite the substrates themselves presenting lower values, i.e., 64 $mJ \cdot m^{-2}$ and 56 $mJ \cdot m^{-2}$, respectively. Conversely, the films cast on copper displayed a significantly diminished SFE, registering 48 $mJ \cdot m^{-2}$ for the top surface, 35 $mJ \cdot m^{-2}$ for the bottom surface, and 48 $mJ \cdot m^{-2}$ for the bulk material. These findings underscore the substrate's influence on both the top and bottom film layers, impacting surface energy. This observation carries substantial implications for applications such as printing, where elevated SFE values are paramount. Enhanced SFE facilitates improved ink wetting, as effective adhesion necessitates the ink's surface tension to be lower than the substrate's SFE.

Microscopic imaging did not indicate a substrate-dependent morphology of the top film layer, as expected. However, the bottom layer exhibited substantial variations. Glass yielded a nearly transparent surface with minimal irregularities. Laminate displayed a more ordered bottom surface compared to the top, albeit without discernible patterns or structures. The films cast on copper exhibited micro-striations, potentially accounting for their enhanced adhesion. The films cast on Teflon replicated the substrate's surface imperfections. This suggests the potential for controlled microstructuring techniques using Teflon®-based templates, which could be useful in specialized optical or electronic applications. The cross-sectional analysis of the film cast on Teflon® (Figure 9) revealed a reticulated structure, reminiscent of leaf venation, which is particularly discernible at higher magnification (b). A wider field of view (a) reveals discontinuities along the edge, likely due to fragment detachment during sectioning. We hypothesize that this structure is a consequence of the desiccation process, which is more stochastic on Teflon due to diminished surface adhesion. These findings are of significant interest.

Scanning electron microscopy (SEM) imaging corroborated the findings obtained from optical microscopy. The microstructures observed under standard optical microscopy were also discernible in the SEM images. However, SEM imaging provided more definitive results by eliminating issues related to light reflection, which can introduce artifacts in optical microscopy. Additionally, SEM imaging offered some insights into the film edge characteristics, although the most comprehensive edge information was derived from the cross-sectional images of the films.

The optical properties of the films, particularly transparency, were markedly substrate-dependent. The films cast on glass and laminate displayed higher transparency, likely due to the lower roughness of these substrates and reduced light scattering. Significant color variations were also observed, particularly in the films cast on copper, which exhibited the most pronounced $\Delta Lab$ shifts. Variations in water vapor permeability were observed, though these differences did not reach statistical significance. This confirms that bulk material properties play a more dominant role in vapor resistance than surface characteristics. While not statistically significant, these findings corroborate observations from other studies, underscoring the importance of considering substrate effects in starch-based film research.

In summary, this study revealed a significant impact of substrate type on the surface properties of starch-based films, including optical properties and water vapor permeability. The absence of statistically significant differences in tensile strength under static conditions does not exclude potential substrate influences on other mechanical properties. Further

investigations should include dynamic mechanical testing to determine the impact of drying-induced stresses and substrate interactions on films' functional performance. Expanding this research to industrial-scale production methods will be crucial for bridging the gap between laboratory findings and commercial applications.

## 5. Conclusions

This study shows that substrate choice significantly affects starch-based films' structural, optical, and adhesive properties. The casting process on different surfaces led to changes in surface roughness, adhesion strength, and overall film morphology, highlighting the importance of substrate choice in optimizing biodegradable film properties.

The films cast on glass and laminate substrates showed the most homogeneous structures, with relatively high transparency and well-balanced adhesion properties, making them suitable candidates for controlled film formation. Copper substrates, in contrast, induced strong adhesion that prevented removal of the intact films, probably due to the microcracks observed in the bottom layer of the films. Meanwhile, Teflon® substrates induced weak adhesion, leading to spontaneous peeling, but introduced surface irregularities that can be exploited for specific applications, such as microstructuring techniques.

Despite significant differences in adhesion and surface characteristics, mechanical tests showed no statistically significant differences in the tensile strength of the films poured on the different substrates. However, the lower elongation values observed for Teflon cast films suggest a potential effect of drying conditions on mechanical properties. In addition, the water vapor permeability tests showed no significant effects of substrate type on this parameter, suggesting that bulk material properties play a dominant role in moisture resistance.

The optical properties of the films were also found to depend on the substrate, with noticeable color changes on copper surfaces and varying degrees of transparency dependent on surface roughness. These findings have implications for applications where color stability or light transmission is a critical factor.

While this study provides valuable insight into the substrate-dependent behavior of starch-based films, further research is needed to investigate dynamic mechanical properties, long-term environmental stability, and the potential impact of surface modification on film adhesion and performance. Moreover, extending these findings to industrial-scale production methods could help bridge the gap between laboratory research and commercial applications in food packaging, pharmaceutical coatings, and biodegradable electronics.

**Author Contributions:** Conceptualization, T.T.M., Z.Ż.-T. and J.S.; methodology, T.T.M.; validation, J.S. and T.T.M.; formal analysis, J.S. and T.T.M.; investigation, T.T.M.; data curation, T.T.M. and J.S.; writing—original draft preparation, T.T.M. and J.S.; writing—review and editing, J.S. and Z.Ż.-T.; supervision, J.S. All authors have read and agreed to the published version of the manuscript.

**Funding:** This research received no external funding.

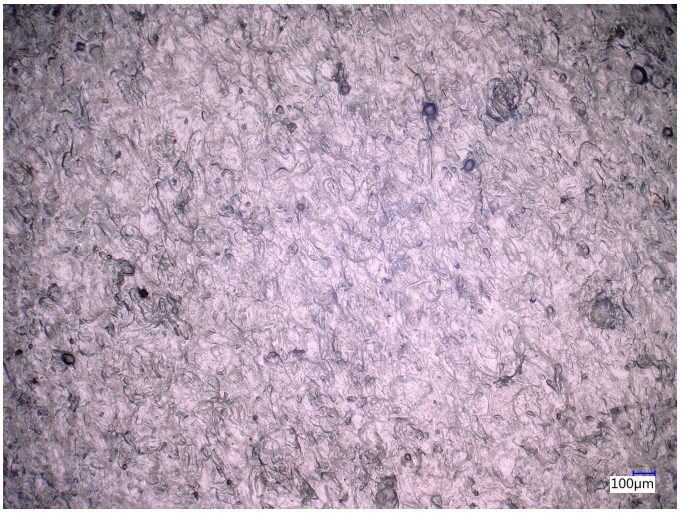
**Data Availability Statement:** The original contributions presented in this study are included in the article. Further inquiries can be directed toward the corresponding author.

**Conflicts of Interest:** The authors declare no conflicts of interest.

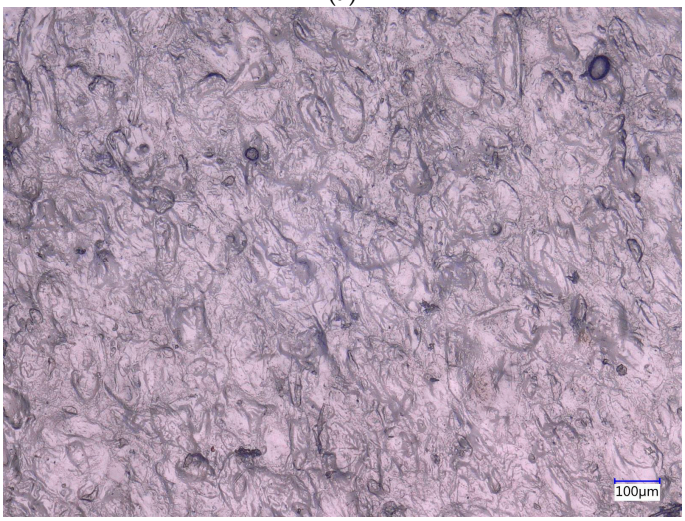
## Appendix A

Below are microscope images of the film surfaces at approximately 100, 200 and 500× magnification.

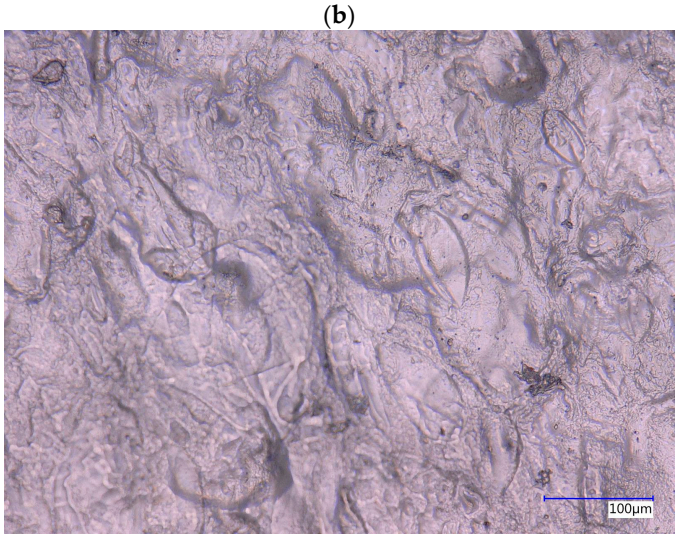
*Appendix A.1*




(**a**)



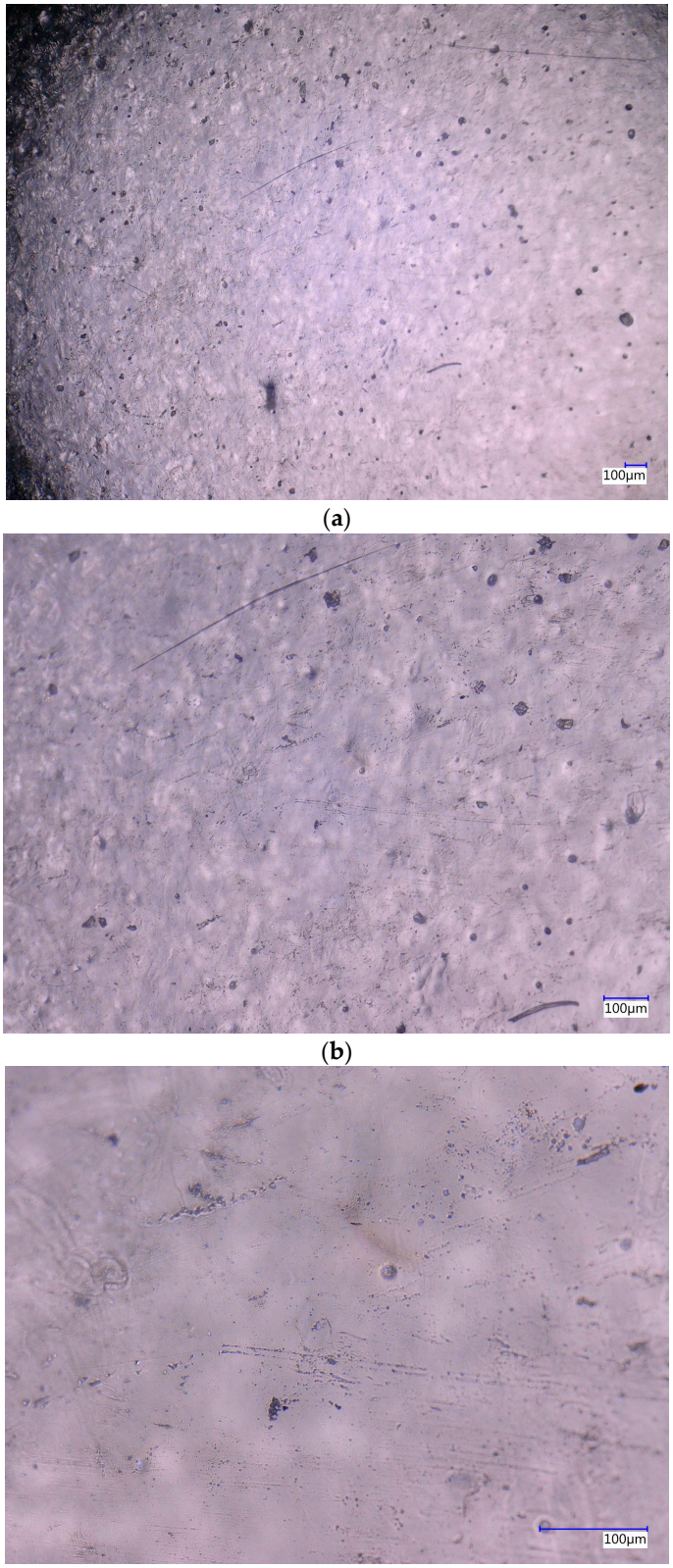

(**b**)




(**c**)

**Figure A1.** Microscopic images of the top film layer obtained on the glass surface with an optical zoom of 100 (**a**), 200 (**b**), and 500 (**c**).

*Appendix A.2*




(**a**)

(**b**)

(**c**)

**Figure A2.** Microscopic images of the bottom film layer obtained on the glass surface with an optical zoom of 100 (**a**), 200 (**b**), and 500 (**c**).

*Appendix A.3*

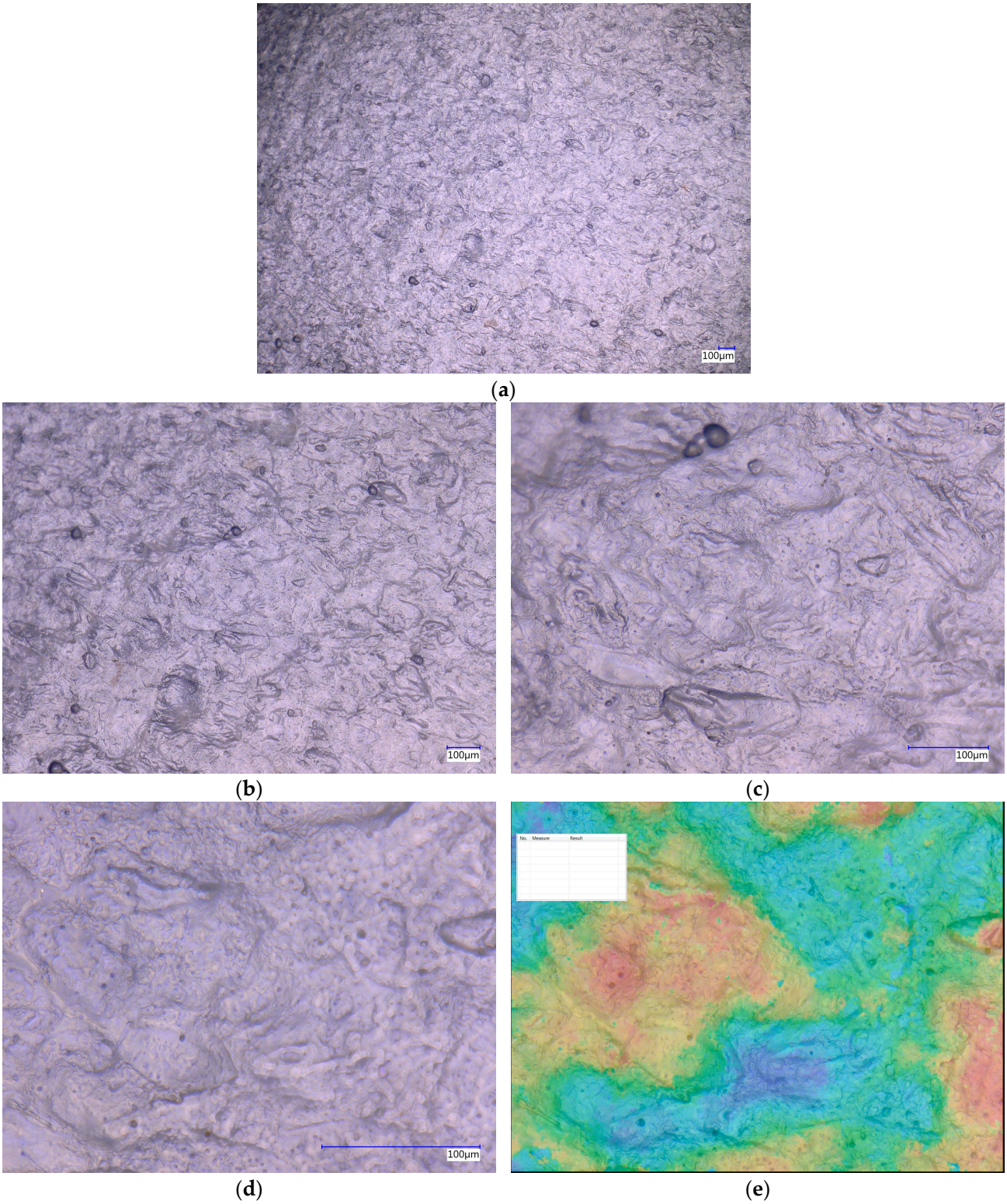
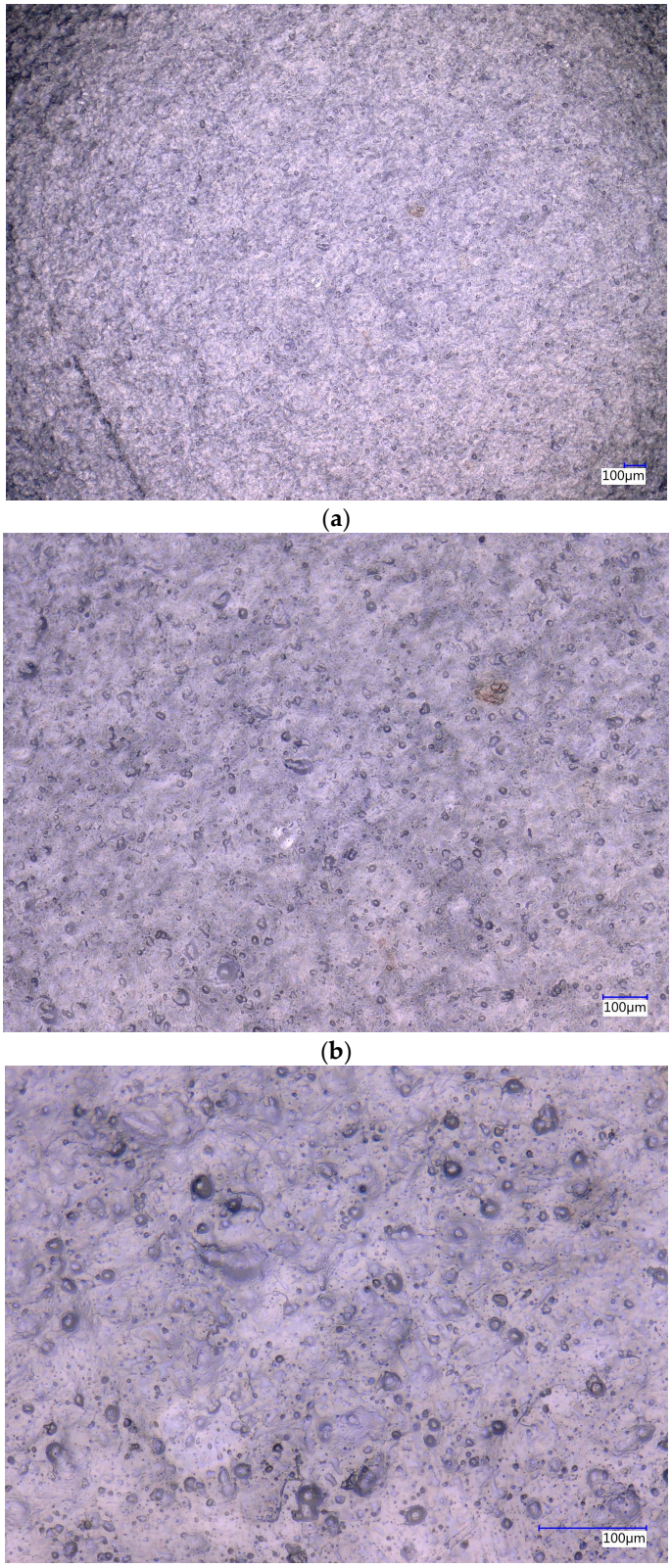



**Figure A3.** Microscopic images of the top film layer obtained on the laminate surface with an optical zoom of 100 (**a**), 200 (**b**), 500 (**c**), and 1000 (**d**) and a height map (**e**), red indicates the highest points, blue the lowest.

*Appendix A.4*



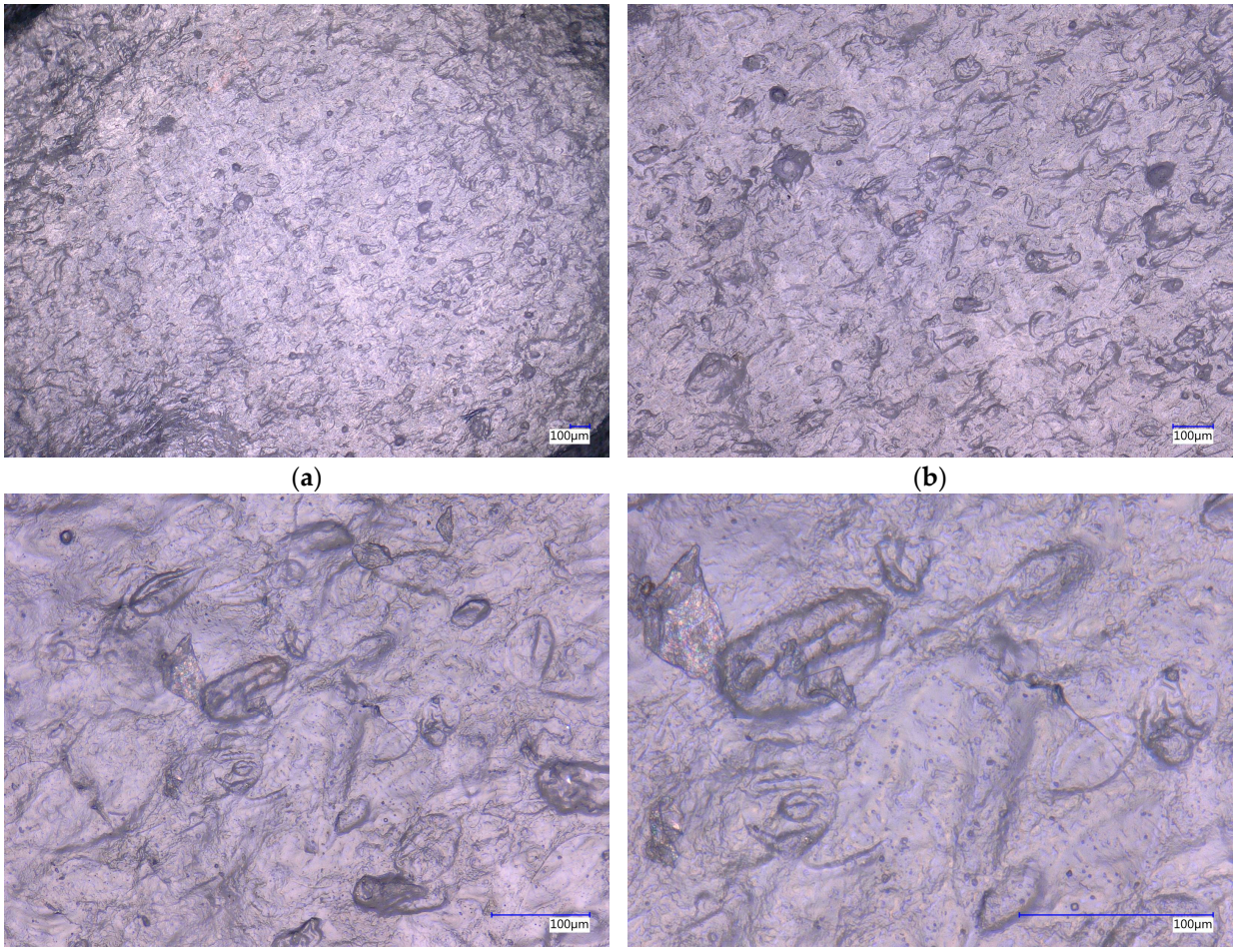

(**a**)

(**b**)

(**c**)

**Figure A4.** Microscopic images of the bottom film layer obtained on the laminate surface with an optical zoom of 100 (**a**), 200 (**b**), and 500 (**c**).

*Appendix A.5*

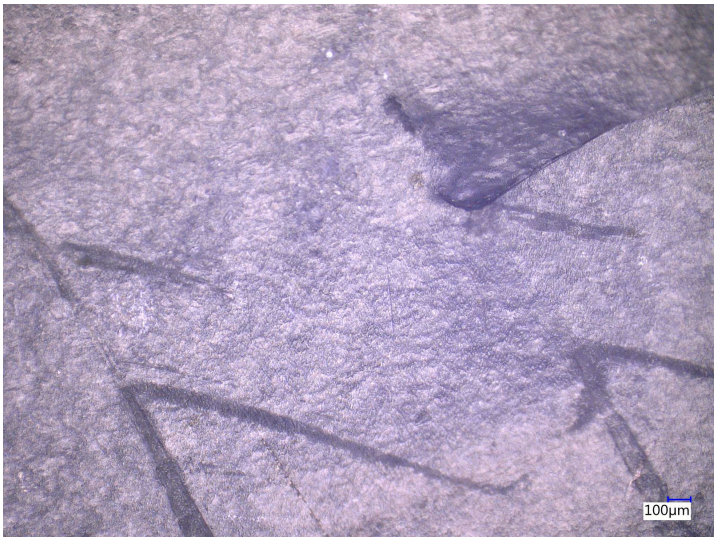



(**a**) (**b**)

(**c**) (**d**)

**Figure A5.** Microscopic images of the top film layer obtained on the copper surface with an optical zoom of 100 (**a**), 200 (**b**), 500 (**c**), and 1000 (**d**).

*Appendix A.6*

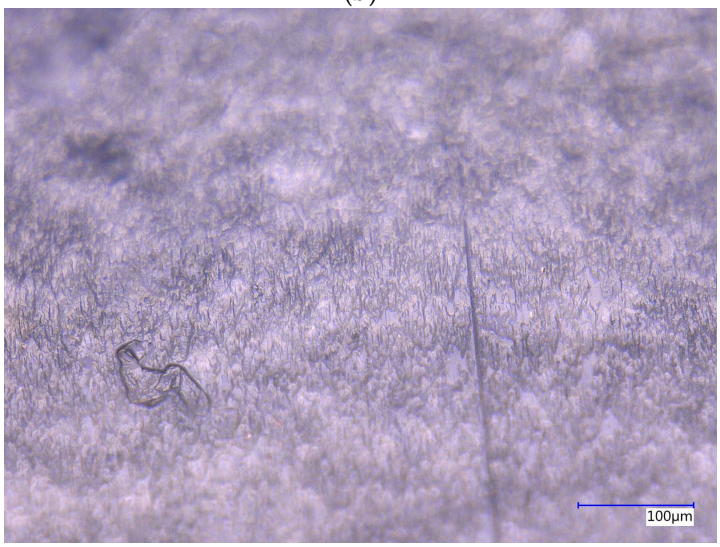



(**a**)

**Figure A6.** *Cont.*



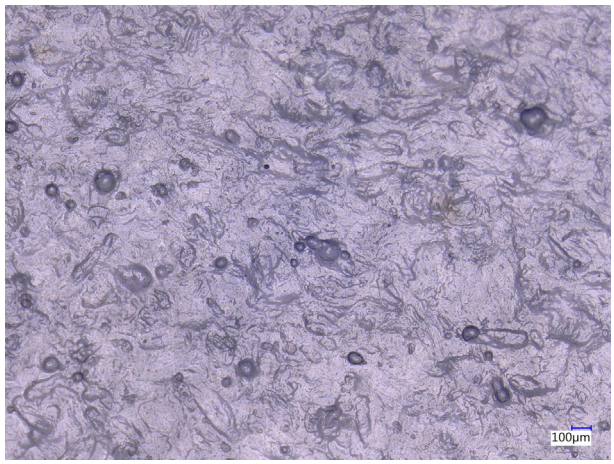

(**b**)




(**c**)

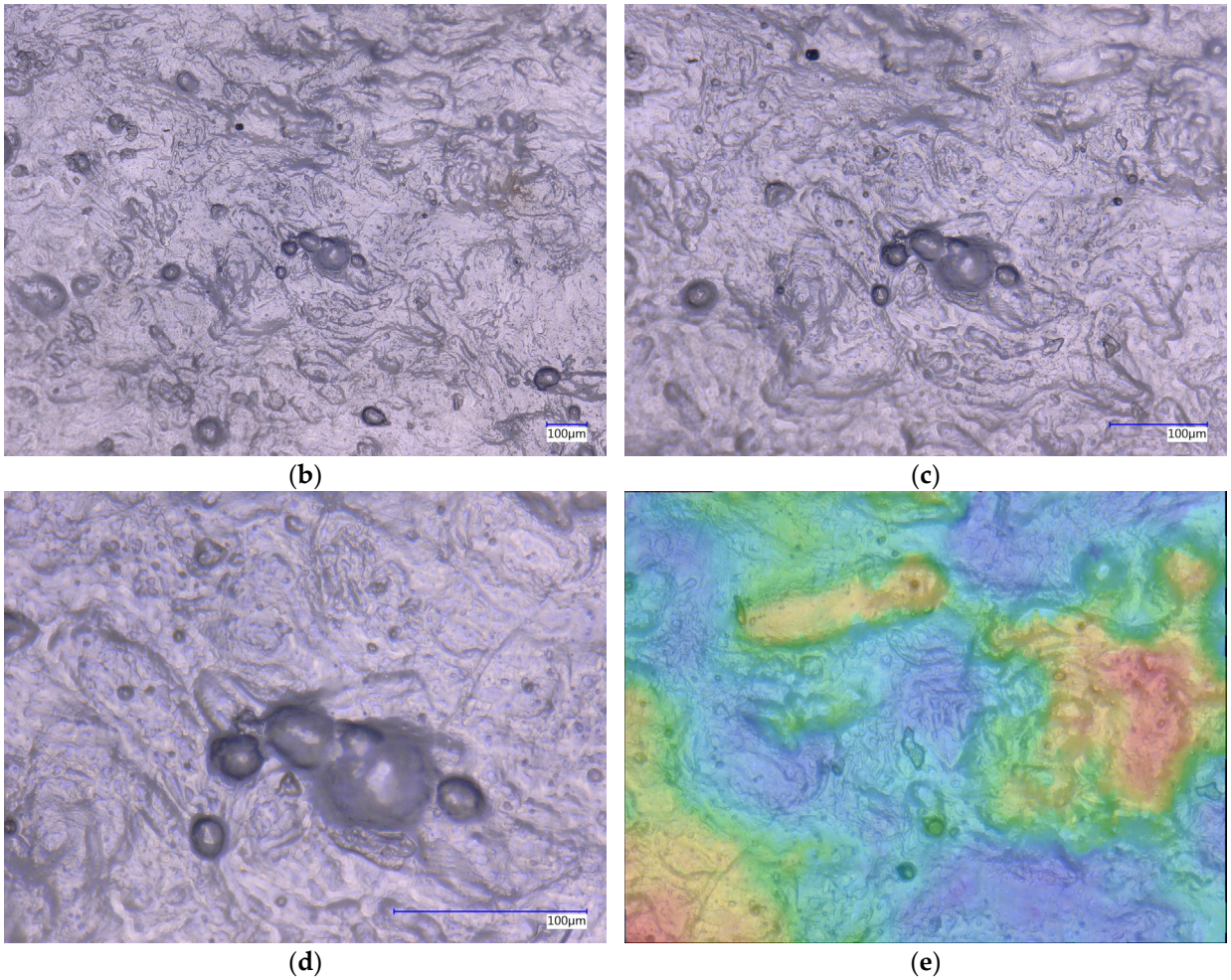
**Figure A6.** Microscopic images of the bottom film layer obtained on the copper surface with an optical zoom of 100 (**a**), 200 (**b**), and 500 (**c**).

*Appendix A.7*




(**a**)

**Figure A7.** *Cont.*

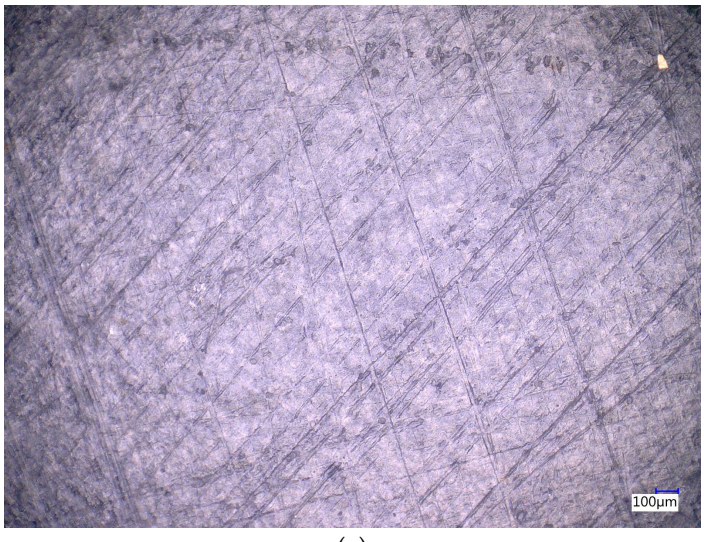



(**b**) (**c**)

(**d**) (**e**)

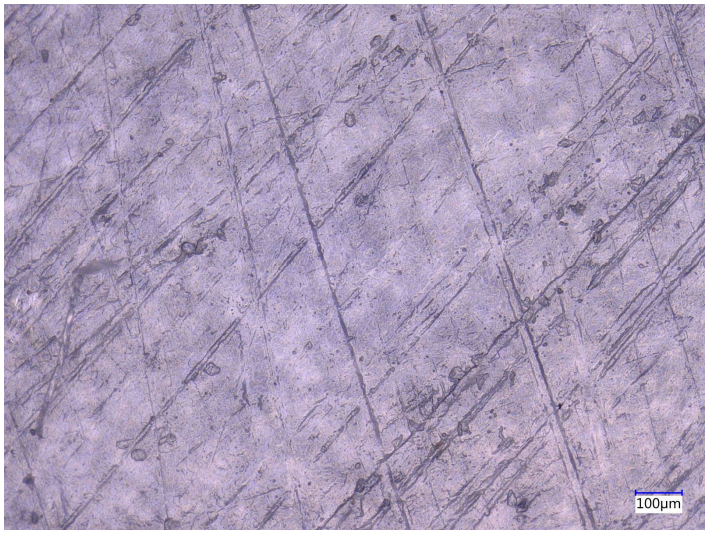
**Figure A7.** Microscopic images of the top film layer obtained on the Teflon surface with an optical zoom of 100 (**a**), 200 (**b**), 500 (**c**), and 1000 (**d**) and a height map (**e**), red indicates the highest points, blue the lowest.

*Appendix A.8*

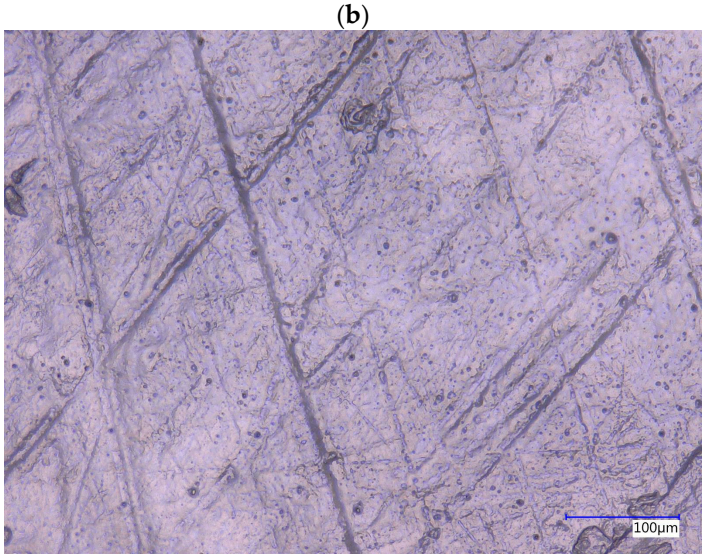



(**a**)

**Figure A8.** *Cont.*



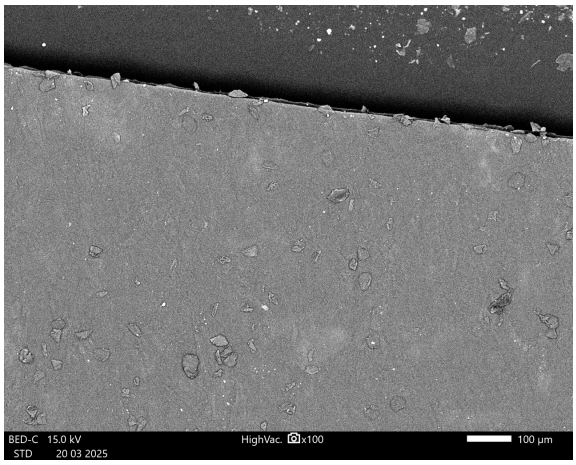

(**b**)



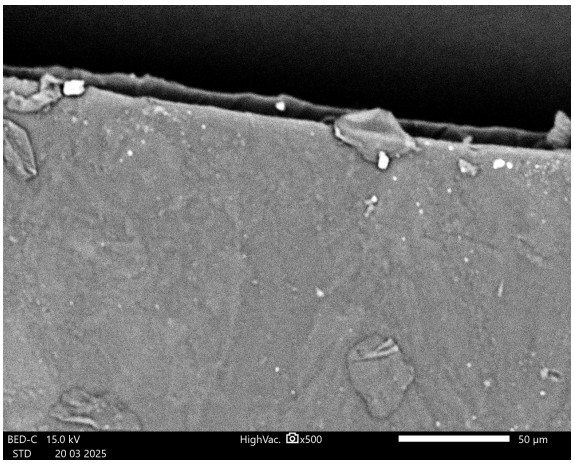

(**c**)

**Figure A8.** Microscopic images of the bottom film layer obtained on the Teflon surface with an optical zoom of 100 (**a**), 200 (**b**), and 500 (**c**).

*Appendix A.9*



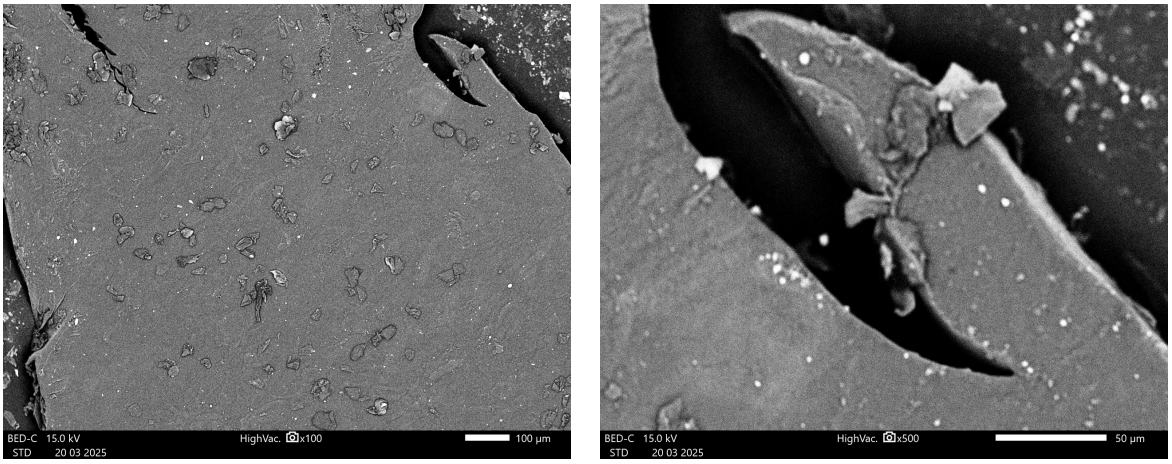

(**a**)




(**b**)

**Figure A9.** SEM images of the top film layer obtained on the Laminate surface with an optical zoom of 100 (**a**)and 500 (**b**).

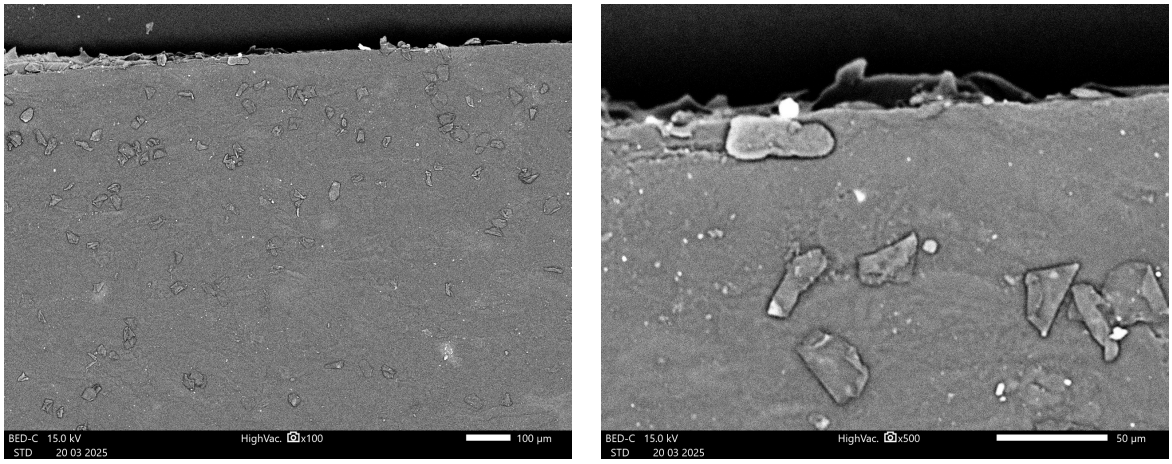
*Appendix A.10*




(**a**) (**b**)

**Figure A10.** Scanning electron microscopy (SEM) images of a film cast on copper are presented, showcasing the top layer at magnifications of 100× (**a**) and 500× (**b**).

*Appendix A.11*




(**a**) (**b**)

**Figure A11.** Scanning electron microscopy (SEM) images of a film cast on Teflon are presented, showcasing the top layer at magnifications of 100× (**a**) and 500× (**b**).

## References

1. Dirpan, A.; Ainani, A.F.; Djalal, M. A Review on Biopolymer-Based Biodegradable Film for Food Packaging: Trends over the Last Decade and Future Research. *Polymers* **2023**, *15*, 2781. [CrossRef]
2. Díaz-Montes, E. Polysaccharide-Based Biodegradable Films: An Alternative in Food Packaging. *Polysaccharides* **2022**, *3*, 761–775. [CrossRef]
3. Giatrakou, V.I.; Al-Daour, R.; Savvaidis, I.N. Chitosan and Hurdle Technologies to Extend the Shelf Life or Reassure the Safety of Food Formulations and Ready-to-Eat/Cook Preparations/Meals. In *Chitosan: Novel Applications in Food Systems*; Martelli-Tosi, M.A., de la Torre, A.R., Klein, E.J., Eds.; Academic Press: Cambridge, MA, USA, 2023; pp. 189–210. [CrossRef]
4. Benalaya, I.; Alves, G.; Lopes, J.; Silva, L.R. A Review of Natural Polysaccharides: Sources, Characteristics, Properties, Food, and Pharmaceutical Applications. *Int. J. Mol. Sci.* **2024**, *25*, 1322. [CrossRef] [PubMed]
5. Lisitsyn, A.; Semenova, A.; Nasonova, V.; Polishchuk, E.; Revutskaya, N.; Kozyrev, I.; Kotenkova, E. Approaches in Animal Proteins and Natural Polysaccharides Application for Food Packaging: Edible Film Production and Quality Estimation. *Polymers* **2021**, *13*, 1592. [CrossRef] [PubMed]
6. Kuorwel, K.K.; Cran, M.J.; Sonneveld, K.; Miltz, J.; Bigger, S.W. Antimicrobial Activity of Biodegradable Polysaccharide and Protein-Based Films Containing Active Agents. *J. Food Sci.* **2011**, *76*, R90–R102. [CrossRef]

7. Mohamed, S.A.A.; El-Sakhawy, M.; El-Sakhawy, M.A.M. Polysaccharides, Protein and Lipid -Based Natural Edible Films in Food Packaging: A Review. *Carbohydr. Polym.* **2020**, *238*, 116178. [CrossRef]
8. Versino, F.; Ortega, F.; Monroy, Y.; Rivero, S.; López, O.V.; García, M.A. Sustainable and Bio-Based Food Packaging: A Review on Past and Current Design Innovations. *Foods* **2023**, *12*, 1057. [CrossRef] [PubMed]
9. Baghi, F.; Gharsallaoui, A.; Dumas, E.; Ghnimi, S. Advancements in Biodegradable Active Films for Food Packaging: Effects of Nano/Microcapsule Incorporation. *Foods* **2022**, *11*, 760. [CrossRef]
10. Shah, Y.A.; Bhatia, S.; Al-Harrasi, A.; Khan, T.S. Advancements in the biopolymer films for food packaging applications: A short review. *Biotechnol. Sustain. Mater.* **2024**, *1*, 2. [CrossRef]
11. Manzoor, A.; Khan, S.; Dar, A.H.; Pandey, V.K.; Shams, R.; Ahmad, S.; Jeevarathinam, G.; Kumar, M.; Singh, P.; Pandiselvam, R. Recent insights into green antimicrobial packaging towards food safety reinforcement: A review. *J. Food Saf.* **2024**, *43*, e13046. [CrossRef]
12. Deshmukh, R.K.; Gaikwad, K.K. Natural antimicrobial and antioxidant compounds for active food packaging applications. *Biomass-Convers. Biorefinery* **2024**, *14*, 4419–4440. [CrossRef]
13. Ncube, L.K.; Ude, A.U.; Ogunmuyiwa, E.N.; Zulkifli, R.; Beas, I.N. Environmental Impact of Food Packaging Materials: A Review of Contemporary Development from Conventional Plastics to Polylactic Acid Based Materials. *Materials* **2020**, *13*, 4994. [CrossRef] [PubMed]
14. European Commission. European Strategy for Plastics in a Circular Economy. 2018. Available online: https://eur-lex.europa.eu/legal-content/EN/TXT/?uri=CELEX:52018DC0028 (accessed on 30 January 2025).
15. European Parliament and Council. Directive (EU) 2019/904 on the Reduction of the Impact of Certain Plastic Products on the Environment. 2019. Available online: https://eur-lex.europa.eu/legal-content/EN/TXT/?uri=CELEX:32019L0904 (accessed on 30 January 2025).
16. European Parliament and Council. Regulation (EU) 2025/40 on Packaging and Packaging Waste. 2025. Available online: https://eur-lex.europa.eu/eli/reg/2025/40/oj/eng (accessed on 30 January 2025).
17. Motelica, L.; Ficai, D.; Ficai, A.; Oprea, O.C.; Kaya, D.A.; Andronescu, E. Biodegradable Antimicrobial Food Packaging: Trends and Perspectives. *Foods* **2020**, *9*, 1438. [CrossRef] [PubMed]
18. Hernández-García, E.; Vargas, M.; González-Martínez, C.; Chiralt, A. Biodegradable Antimicrobial Films for Food Packaging: Effect of Antimicrobials on Degradation. *Foods* **2021**, *10*, 1256. [CrossRef] [PubMed]
19. Saeed, K.; Ali, Z. Biodegradable meat packaging: Microbial safety and control for environmental pollution. *Theory Pr. meat Process.* **2024**, *9*, 169–179. [CrossRef]
20. Zhao, Y.; Sun, H.; Yang, B.; Weng, Y. Hemicellulose-Based Film: Potential Green Films for Food Packaging. *Polymers* **2020**, *12*, 1775. [CrossRef]
21. Hussain, S.A.; Yadav, M.P.; Sharma, B.K.; Qi, P.X.; Jin, T.Z. Biodegradable Food Packaging Films Using a Combination of Hemicellulose and Cellulose Derivatives. *Polymers* **2024**, *16*, 3171. [CrossRef]
22. Bhalsing, P.; Verma, P. Smart Packaging for Sustainable Food Waste Management: A Review. *Eur. J. Nutr. Food Saf.* **2024**, *16*, 290–299. [CrossRef]
23. Li, S.; Ren, Y.; Hou, Y.; Zhan, Q.; Jin, P.; Zheng, Y.; Wu, Z. Polysaccharide-Based Composite Films: Promising Biodegradable Food Packaging Materials. *Foods* **2024**, *13*, 3674. [CrossRef]
24. Abral, H.; Basri, A.; Muhammad, F.; Fernando, Y.; Hafizulhaq, F.; Mahardika, M.; Sugiarti, E.; Sapuan, S.; Ilyas, R.; Stephane, I. A simple method for improving the properties of the sago starch films prepared by using ultrasonication treatment. *Food Hydrocoll.* **2019**, *93*, 276–283. [CrossRef]
25. Żołek-Tryznowska, Z.; Jeznach, A.; Bednarczyk, E.; Tryznowski, M. Influence of Ultrasonic Treatment on the Mechanical and Surface Properties of Potato Starch-Based Films with Various Glycerol Content. *GRID* **2024**, *9*, 169–179. [CrossRef]
26. Gyawali, K.; Ghimire, P.; Bhandari, A. A Study on Synthesis and Characterization of Bio-Plastic Obtained from Potato. *Am. J. Chem. Pharm.* **2024**, *3*, 20–26. [CrossRef]
27. Grewell, D.; Travalini, A.; Demiate, I.; Lamsal, B. Starch-Based Biopolymer Films. In *Biopolymer-Based Materials for Food Packaging Applications*; Royal Society of Chemistry: London, UK, 2023; Chapter 9. [CrossRef]
28. Bajer, D. Eco-Friendly, Biodegradable Starch-Based Packaging Materials with Antioxidant Features. *Polymers* **2024**, *16*, 958. [CrossRef]
29. Garbarski, J.; Fabijański, M. Application of a Filler in the Form of Micronized Chalcedonite to Biodegradable Materials Based on Thermoplastic Starch as an Element of the Sustainable Development of Polymeric Materials. *Sustainability* **2025**, *17*, 2731. [CrossRef]
30. Lepak-Kuc, S.; Kądziela, A.; Staniszewska, M.; Janczak, D.; Jakubowska, M.; Bednarczyk, E.; Murawski, T.; Piłczyńska, K.; Żołek-Tryznowska, Z. Sustainable, cytocompatible and flexible electronics on potato starch-based films. *Sci. Rep.* **2024**, *14*, 18838. [CrossRef]

31. Bartnik, J.P.; Nehru, D.; Motadayen, M.; Agarwala, S. Biodegradable Temperature Sensor enabled using Printed Electronics. In Proceedings of the 2024 IEEE International Conference on Flexible and Printable Sensors and Systems (FLEPS), Tampere, Finland, 30 June–3 July 2024; pp. 1–4.
32. Hemanth, B.; Meghashree, M.; Sanjay, P.K.; Kalungade, R.R. Edible Electronics for Smart Technology Solutions: Edible Electronics for Food Packaging. In *Edible Electronics for Smart Technology Solutions*; Mehta, S., Al-Turjman, F., Eds.; IGI Global: Hershey, PA, USA, 2025; pp. 1–22. [CrossRef]
33. El Guerraf, A.; Ziani, I.; Ben Jadi, S.; El Bachiri, A.; Bazzaoui, M.; Bazzaoui, E.A.; Sher, F. Smart conducting polymer innovations for sustainable and safe food packaging technologies. *Compr. Rev. Food Sci. Food Saf.* **2024**, *23*, e70045. [CrossRef]
34. Tshamisane, M.; Adeyemi, J.O.; Fawole, O.A. Fabrication of active and intelligent bio-based edible films using encapsulated beetroot powders for smart packaging. *Mater. Adv.* **2025**, *6*, 1051–1066. [CrossRef]
35. Ashiwaju, B.I.; Orikpete, O.F.; Fawole, A.A.; Alade, E.Y.; Odogwu, C. A Step toward Sustainability: A Review of Biodegradable Packaging in the Pharmaceutical Industry. *Matrix Sci. Pharma* **2023**, *7*, 73–84. [CrossRef]
36. Gupta, V.; Biswas, D.; Roy, S. A Comprehensive Review of Biodegradable Polymer-Based Films and Coatings and Their Food Packaging Applications. *Materials* **2022**, *15*, 5899. [CrossRef]
37. Kramar, A.; Ortega, I.R.; González-Gaitano, G.; González-Benito, J. Solution casting of cellulose acetate films: Influence of surface substrate and humidity on wettability, morphology and optical properties. *Cellulose* **2023**, *30*, 2037–2052. [CrossRef]
38. Yang, J.; Huang, Y.; Xu, K. Effect of substrate on surface morphology evolution of Cu thin films deposited by magnetron sputtering. *Surf. Coatings Technol.* **2007**, *201*, 5574–5577. [CrossRef]
39. Filatova, E.O.; Peverini, L.; Ziegler, E.; Kozhevnikov, I.V.; Jonnard, P.; André, J.-M. Evolution of surface morphology at the early stage of $Al_2O_3$ film growth on a rough substrate. *J. Phys. Condens. Matter* **2010**, *22*, 345003. [CrossRef] [PubMed]
40. Hazra, S.; Gibaud, A.; Sella, C. Influence of substrate roughness on the layering of particles in nanocermet thin films. *J. Phys. D Appl. Phys.* **2001**, *34*, 1575–1578. [CrossRef]
41. *PN-EN ISO 527-3:2019-01*; Plastics—Determination of tensile properties—Part 3: Test Conditions for Films and Plates. Polish Committee for Standardization: Warsaw, Poland, 2019.
42. *ISO 15989:2004*; Plastics—Film and Sheeting—Measurement of Water-Contact Angle of Corona-Treated Films. International Organization for Standardization: Geneva, Switzerland, 2004.
43. Owens, D.K.; Wendt, R.C. Estimation of the surface free energy of polymers. *J. Appl. Polym. Sci.* **1969**, *13*, 1741–1747. [CrossRef]
44. Wu, Y.; Gao, S.; Zhao, J.; Kong, S.; Wang, H.; Wang, W.; Hou, H. Sugar/sugar alcohol with glycerol as co-plasticizers for high-content starch/PBAT blown films: From fine structure to physicochemical properties. *J. Sci. Food Agric.* **2025**, *105*, 1105–1115. [CrossRef]


**Disclaimer/Publisher's Note:** The statements, opinions and data contained in all publications are solely those of the individual author(s) and contributor(s) and not of MDPI and/or the editor(s). MDPI and/or the editor(s) disclaim responsibility for any injury to people or property resulting from any ideas, methods, instructions or products referred to in the content.